Ph.D. Dissertation of Medical Science

Development of immunotherapy for viral diseases by regulating macrophages-mediated cytokines

마크로파지 매개 사이토카인 조절을 통한 바이러스 면역 치료제 개발 연구

February 2023

Seoul National University College of Medicine
Department of Microbiology and Immunology

Jung Won Kwon

Development of immunotherapy for viral diseases by regulating macrophages-mediated cytokines

Advisor: Prof. Seung Hyeok Seok

Submitting a Ph.D. Dissertation of
Medicine

October 2022

Seoul National University College of Medicine
Department of Microbiology and Immunology

Jung Won Kwon

Confirming the Ph.D. Dissertation written by
Jung Won Kwon

January 2023

Chair	_____(Seal)
Vice Chair	_____(Seal)
Examiner	_____(Seal)
Examiner	_____(Seal)
Examiner	_____(Seal)

ABSTRACT

Development of immunotherapy for viral diseases by regulating macrophages-mediated cytokines

Jung Won Kwon
Department of Microbiology and Immunology
The Graduate School
Seoul National University College of Medicine

Macrophages are an essential component of innate cellular immunity with flexible functions prominently involved in host defense and immunity against foreign microorganisms, including bacteria, viruses, and fungi. Many viruses target macrophages, and activated macrophages lead to phagocytosis and the release of pro-inflammatory cytokines and chemokines. However, excessive secretion of pro-inflammatory cytokines by macrophages contributes to local tissue damage and a dangerous systemic inflammatory response. Since monocytes and macrophages are the central cells that secrete pro-inflammatory cytokines, the efficient control of these cells can be used as a therapeutic target to regulate cytokines. In this study, I aimed to regulate influenza virus-mediated hyper-inflammation by targeting macrophages and then examined the immune mechanism regulating interleukin (IL)-12 in macrophages during dengue virus infection. First, in this study, I developed liposomes that are selectively delivered to macrophages. Also, I found that liposomal dexamethasone (DEX/lipo) significantly reduced the protein level of tumor necrosis factor-alpha (TNF-α), IL-1β, IL-6, and the C-X-C motif

chemokine ligand 2 (CXCL2) as well as the number of infiltrated immune cells in the bronchoalveolar lavage fluids as compared to the control and free dexamethasone (DEX) in influenza virus-infected mice. Moreover, the intranasal delivery of DEX/lipo during disease progression reduced the death rate by 20%. Therefore, the intranasal delivery of DEX/lipo may serve as a novel promising therapeutic strategy for treating influenza virus-induced pneumonia (Chapter 1). Next, I revealed the cause of decreased IL-12 after severe dengue virus infection in macrophages through dengue virus binding receptor-mediated signaling. As a result, in type I interferon receptor knockout (IFNAR KO) mice infected with severe dengue virus, down-regulated IL-12 decreased vessel tight junction through increasing matrix metalloproteinase-9 (MMP-9). In addition, I found that mice treated with recombinant IL-12 rapidly regained body weight and attenuated dengue hemorrhagic fever. Based on a reliable model, I have developed a potential therapeutic strategy to attenuate dengue hemorrhagic fever (Chapter 2). Together, my results provide valuable insights into the development of immunotherapies for viral disease via regulating cytokines by targeting macrophages.

* This dissertation is based on previously published articles.

Jung Won Kwon *et al.* (2022) *Frontiers in Microbiology*, 13:845795.

Keywords: Macrophages, Immunotherapy, Influenza virus, Dengue virus, Cytokines, Liposome
Student Number: 2016-21898

GENERAL INTRODUCTION

Cytokines are small and secreted protein-based cell signaling molecules that include cell-to-cell communication, cell activation, differentiation, and stimulation of other cells to the sites of inflammation, infection, and trauma (1). Viral infections induce a pro-inflammatory response, including the expression of cytokines and chemokines (2, 3). As a result, the subsequent immune cell recruitment and antiviral effector functions contribute to the first line of defense against viruses. However, excessive cytokines and chemokines can cause serious immune pathology. Uncontrolled systemic inflammation characterized by high concentrations of pro-inflammatory cytokines and chemokines are potentially harmful in the course of viral infections. For example, deaths caused by severe influenza are usually related to cytokine storms (4, 5).

Macrophages play multiple roles in the innate immune system. They can phagocytose bacteria and viruses to trigger an immune response, as well as promote tissue homeostasis and regeneration (6). Cytokines caused by viruses induce the phenotypic programming of these monocyte-derived macrophages, which can be inflammatory macrophages (6, 7). Inflammatory macrophages are associated with microbicidal activity, pro-inflammatory cytokine production, and immune response (7). In addition, they have increased the production of inflammatory mediators, reactive oxygen species, costimulatory molecules, antigen presentation, and phagocytic activity (8).

Many types of viruses (e.g., influenza virus, chikungunya, human herpes, and dengue viruses) can target monocytes/macrophages and cause severe diseases by hyper-inflammation (9-11). For example, in the case of the influenza virus, after the primary infection of respiratory epithelial cells, viremia replicates within these cells and can infect other cells, including alveolar macrophages (12-14). Infected macrophages produce a lot of interleukin (IL)-1α, IL-1β, transforming growth factor-β (TGF-β), tumor necrosis factor-α (TNF-α), IL-6 and interferon (IFN)-α/β (3, 15-17). Meanwhile, activation of the endothelium by the expression of IL-6, IL-8, and TNF-α induced dengue virus infection leads to plasma leakage compromising hemodynamics and coagulopathy (18).

Given the role of inflammation in viral pathogenesis, the use of adjunctive immuno-modulating agents remains a topic of great interest. Passive immunotherapies such as statins, PPAR agonists, and COX-2 inhibitors have demonstrated benefits when administered as an adjunctive therapy for severe influenza virus (14, 19). However, there are also concerns that systemic immunosuppression by administration of anti-inflammation medicine can promote persistent viral replication and further limit host defenses such as secondary infection. Therefore, when monocytes and macrophages seem to be implicated in hyper-inflammation in virus infection (20, 21), macrophages should be analyzed and targeted in viral infection to inhibit systemic hyper-inflammation and alleviate cytokines-mediated severe diseases.

Strategies to target macrophages are growing in importance both

scientifically and therapeutically. As particulate carriers, liposomes naturally target cells of the mononuclear phagocytic cells, particularly macrophages. Therefore, loading drugs into liposomes can offer an efficient means of drug-targeting macrophages. Many other studies manufactured liposomes using physicochemical properties, including size, charge, and lipid composition, targeting specific cell types (22). Also, targeting monocytes/macrophages using liposomes could help treat conditions including cancer, atherosclerosis, viral infection, and chronic inflammation. In this study, I manufactured liposomes with large sizes to target macrophages and confirmed that 1,000 nm-sized liposomes are more effective than 50 nm and 200 nm-sized liposomes.

In the chapter 1 study, I ultimately aimed to target the macrophages regulating cytokines using the liposomal dexamethasone (DEX/lipo) during influenza virus infection. Also, I demonstrated the therapeutic efficacy of DEX/lipo *in vivo* model of influenza virus infection. In addition, I found that DEX/lipo outperformed free dexamethasone (DEX) in reducing the morbidity and mortality caused by the A/H1N1 influenza virus infection.

Globally it is estimated that 3.9 billion people from more than 128 countries are at risk of dengue virus (DV) infection, with 284-528 million cases occurring each year, of which 96 million manifest clinically with a severe form of the disease (23). Clinical features of dengue fever (DF) and dengue hemorrhagic fever (DHF) are diverse and non-specific, causing unpredictable progression and outcomes. Unfortunately, no DV-specific therapies or vaccines are available (24). However, its progression

and severity have been known to be associated with cytokine level alteration (25). Dendritic cells (DCs) and macrophages are the primary targets of DV infections (26). Whereas infected DCs undergo apoptosis, infected macrophages survive for at least 45 days and secrete multiple cytokines and chemokines within 6 hours after infection in target organs (27). This result suggests that macrophages are the primary source of pro-inflammatory cytokines after infection with DV, in which virions might trigger inflammatory reactions by activating pattern recognition receptors, Toll-like receptors (TLRs), C-type lectins and immunoglobulin-like (Ig-like) receptors (for example, TREMs (triggering receptors expressed on myeloid cells)) (28, 29). This unregulated production of pro-inflammatory cytokines can aggravate pathogenesis and organ failure and cause death (30).

The cytokine profile of individual patients with DF showed increased levels of IFN-γ and IL-2 and the absence of IL-4, IL-6, and IL-10, a typical Th1-type response. In contrast, DHF grade IV showed high levels of IL-4, IL-6, and IL-10 and lower levels or absence of IL-2 and IFN-γ, a typical Th2-type response (25). An analysis of total cases showed that 66% of the cases of DF had a Th1-type response. As the severity of the illness increased, lower levels of IL-12 were detected in the sera of patients with DHF (31).

IL-12, mainly produced by monocytes/macrophages in response to infectious agents, profoundly affects the levels of Th1 cells and Th1-type cytokines. Furthermore, IL-12 has been associated with the clearance of

viruses, host recovery, and protection in many viral infections (32). Thus IL-12 might play a role in preventing severe dengue disease by maintaining the Th1-type response. If this is true, IL-12 therapy has a profound beneficial effect on the outcome of severe dengue disease, as seen in several other viral infections.

To find the mechanism by which IL-12 was decreased in severe dengue virus infection, I established two reliable *in vitro* infection models in this study. The first is a method of infection of macrophages with a high viral titer. As a result, the dengue virus was concentrated using an ultracentrifuge, and severe infection conditions were confirmed by increased viral amplification and pro-inflammatory cytokines production. The second method is an antibody-dependent enhancement (ADE) infection of DV. There are serotypes 1-4 of DV, and when viruses of other serotypes are infected, previous antibodies that cannot neutralize different serotypes of viruses and instead enter into cells such as macrophages through the Fc gamma receptors (FcγRs). Also, unneutralized viruses are produced, leading to severe diseases. To follow this phenomenon, in this study, I made an immune complex using antibodies of DV type 3 (αDV3) and DV type 2 (DV2) and infected that with macrophages. I also confirmed increased viral amplification and pro-inflammatory cytokines in ADE of DV infection, thereby mimicking two severe infections *in vitro* conditions.

I started the chapter 2 study with two research questions. 1) Why is IL-12 decreased under severe viral conditions? What mechanisms are

involved? 2) What role does IL-12 play in the pathogenesis of DHF? My study's key finding is investigating human macrophage signaling events involved in the production of IL-12. Here, I identify the C-type lectin domain containing 5A (CLEC5A) and FcγRs as a suppressor of IL-12. This study demonstrates that severe DV infection (e.g., high dose of DV infection or ADE of DV infection) triggered CLEC5A or FcγR, which led to specific degradation of interferon regulatory factor 1 (IRF1), thereby suppressing *IL12A* transcription in macrophages. In addition, CLEC5A and FcγR signaling led to E3 ubiquitin ligase mouse double minute 2 homolog (MDM2)-dependent proteasomal degradation of IRF1 in the nucleus. Furthermore, I reported that high doses of DV infection and ADE of DV infection induced vascular permeability *in vitro* and *in vivo* by down-regulating IL-12 production to induce matrix metalloproteinase-9 (MMP-9).

Therefore, my study offers valuable insights into the efficiency of the currently available immunotherapeutic approach to influenza virus infection and severe dengue virus infection via the targeted inflammatory macrophages.

Table of Contents

LIST OF FIGURES

CHAPTER 1. Liposomal Dexamethasone Reduces Influenza virus-induced Hyper-inflammation in Mice by Targeting Macrophages

CHAPTER 2. Severe Dengue virus Infection-mediated Suppression of IL-12 Reduces Antiviral Response by CLEC5A and FcγR signaling in Macrophages

LIST OF ABBREVIATIONS

TNF-α : tumor necrosis factor-alpha

IL-1β : interleukin-1 β

CXCL2: C-X-C motif chemokine ligand 2

IL-12: interleukin-12

MMP-9: matrix metalloproteinases-9

IFNAR KO: type I interferon receptor knockout

PAMP: pathogen-associated molecular pattern

PRR: pattern recognition receptors

DEX: dexamethasone

DEX/lipo: liposomal dexamethasone

$TCID_{50}$: tissue culture infectious dose 50%

BALF: bronchoalveolar lavage fluid

DLS: dynamic light scattering

DV: dengue virus

MR: mannose receptor

DC-SIGN: dendritic cell-specific intercellular adhesion molecule-3-grabbing non-integrin

CLEC5A: C-type lectin domain family 5 member

ADE: antibody-dependent enhancement

FcγR: Fc-gamma receptors

IRF1: interferon regulatory factor 1

MDM2: mouse double minute 2 homolog

MOI: multiplicity of infection

Syk: spleen tyrosine kinase

PLCγ: phospholipase c gamma

PI3K: phosphoinositide 3-kinase

TLR: toll-like receptors

ITAM: immunoreceptor tyrosine-based activation motif

ITIM: immunoreceptor tyrosine-based inhibitory motif

ZO-1: Zonula occludens-1

E-cadherin: epithelial cadherin

N-cadherin: Neural cadherin

CHAPTER 1

Liposomal Dexamethasone Reduces Influenza virus-induced Hyper-inflammation in Mice by Targeting Macrophages

INTRODUCTION

Cytokines are small and secreted protein-based cell signaling molecules that include cell-to-cell communication, cell activation, differentiation, and stimulation of other cells to the sites of inflammation, infection, and trauma (1). Cytokines are subdivided based on the nature of the immune response and the source of their production. Among them, pro-inflammatory cytokines initiate the inflammatory response, resulting in the host defense against pathogens by mediating the innate immune response (33-35). After the primary infection of respiratory epithelial cells by the influenza virus, viremia replicates within these cells and can infect other cells, including alveolar macrophages (12-14). The inflammatory response begins when the pathogen-associated molecular pattern (PAMP) is recognized by pattern recognition receptors (PRRs) of innate immune cells (36-38). The secretion of pro-inflammatory cytokines leads to the recruitment of neutrophils, monocytes, macrophages, and T cells into the site of infection (13, 14). If infiltrated these cells produce the excessive production of pro-inflammatory cytokines, which leads to aggressive inflammatory responses and insufficient control of anti-inflammatory responses, which contribute to organ failure and other fatalities during influenza virus infection (39-41). Notably, reducing pro-inflammatory cytokine levels is as worthwhile as anti-viral therapies.

In this study, I aim to alleviate hyper-inflammation by delivering DEX/lipo into alveolar macrophages during the influenza virus infection. Dexamethasone, a corticosteroid type, is a steroid hormone class that

exhibits anti-inflammatory activity by binding to the cytoplasmic corticosteroid receptor, which regulates the transcription of anti-inflammatory genes (14, 42). However, the evidence supporting the use of dexamethasone in severe influenza was unclear (43). In addition, immunosuppression resulting from systemic administration of dexamethasone can favor persistent viral replication and further limit host defenses (44). However, Lammers *et al.* recently proposed that targeting alveolar macrophages via the nano-formulation of dexamethasone within liposomes improves the management of respiratory viral infections (45). Liposomes are microscopic phospholipid materials with a bilayered membrane structure that have been successfully applied in clinics as drug carriers (46). It has been known to improve the delivery of drugs to target cells and tissues that play a key role in the acute and progressive phases of many diseases (46). Although dexamethasone nanomedicine has been used as a therapeutic agent for the coronavirus disease 2019 (COVID-19) (45), it has not yet been tested for influenza virus infection in preclinical studies.

Here, I demonstrate the therapeutic efficacy of DEX/lipo in mice model of influenza virus infection. In addition, I manufacture DEX/lipo that can be specifically delivered into macrophages. Also, I found that DEX/lipo outperformed free dexamethasone in reducing the morbidity and mortality caused by the A/H1N1 influenza virus infection. Therefore, my results offer valuable insights into the efficiency of the currently available corticosteroids for the treatment of influenza virus infection via the

targeted delivery of these drugs.

MATERIALS AND METHODS

Animals

Male wild-type C57BL/6J mice (Orient Bio) between 7 weeks of age were used in this study. Animal experiments were conducted at the Institute for Experimental Animals, College of Medicine and cared for according to the Guide for the Care and Use of Laboratory. The study was approved by the Seoul National University Animal Care and Use Committee (accession number SNU-160307-6-1). Mice were housed in cages with constant-flow air exchange, supporting specific pathogen-free conditions.

Adaptation and amplification of influenza virus

Influenza A/Wisconsin/WSLH34939/09 was obtained from the Michael laboratory at the Scripps Research Institute. The C57BL/6J mice were each anesthetized with isoflurane (HANA PHARM CO.), intranasally inoculated with 10^5 tissue culture infective dose 50% ($TCID_{50}$) of influenza A/Wisconsin/WSLH34939/09 virus in a volume of 20 μL. At day 2 post-infection, the lungs from mice were homogenized in the Dulbecco's modified Eagle medium (DMEM) medium with 10% fetal bovine serum (FBS) and 1% penicillin-streptomycin (PS), centrifuged at 9,520 $\times g$ for 10 minutes. The supernatant was stored at -80℃. The first adapted virus was amplified on the Madin-Darby canine kidney (MDCK) cells, and the virus titer was detected using $TCID_{50}$. Briefly, the assay was performed by adding a serial dilution of the virus sample to cells in a 96-well plate.

After incubation, the percentage of infected wells was observed for each dilution, and the results were used to calculate the $TCID_{50}$ value. This calculation can generally be performed using the Spearman-Karber method.

Cell line culture

MDCK cells were cultured in DMEM supplemented with 10% FBS and 1% PS. Mice under isoflurane anesthesia were infected intranasally with 10^5 $TCID_{50}$ of the adapted influenza A virus. One hour after infection, the mice were anesthetized by isoflurane inhalation for the intranasal delivery of vehicle (20 μL of PBS/lipo) or dexamethasone (30 μg/kg dissolved in PBS) or DEX/lipo (30 μg/kg encapsulated in liposomes) for 3 days. On day 3 post-infection, the mice were injected intravenously with 100 μL of PBS/lipo, dexamethasone, or DEX/lipo. The mice were monitored for survival.

Preparation of liposomes

Dexamethasone (Sigma-Aldrich) was encapsulated into liposomes with a diameter of 1,000 nm at a 1 mg/mL concentration. Briefly, L-alpha-phosphatidylcholine (Sigma-Aldrich) and cholesterol (Sigma-Aldrich) were dissolved in a 2:1 mixture of chloroform and methanol and dried under a nitrogen stream, followed by a vacuum pump. The lipid film was hydrolyzed with PBS buffer and sized to 1,000 nm in a mini-extruder equipped with a 1,000 nm pore polycarbonate membrane (Avanti Polar Lipids). The diameter of liposomes was checked by dynamic light

scattering (DLS). In addition, liposomes were labeled with DiI (Molecular Probes) for visual detection.

Flow cytometry

The mice lungs were obtained at 24 hours post-infection with DiI-stained liposomes and digested with collagenase type I (Sigma-Aldrich) to obtain single cells. Single cells were prepared for flow cytometric analysis. Anti-mouse CD16/32 antibody (clone number 93) was pre-added to block the non-specific binding of the immunoglobulin to macrophage Fc receptors. For surface marker analysis, live cells were re-suspended in staining buffer (1% bovine serum albumin (BSA), 5 mM ethylenediaminetetraacetic acid (EDTA), and 0.1% NaN3 in PBS) and stained with anti-mouse CD45 (30-F11), F4/80 (BM8), CD11b (M1/70), CD3 (145-2C11), CD64 (X54-5/7.1; BD Biosciences), Ly6C (HK1.4), and Ly6G (1A8-Ly6g) antibodies at 4℃ for 20 minutes. All antibodies were obtained from eBioscience unless otherwise indicated. Data were acquired using LSR Fortessa (BD Biosciences) and analyzed using the FlowJo software (FlowJo LCC.).

Immunofluorescence (IF)

The mice lungs were obtained at 24 hours post-infection with DiI-stained liposomes. Frozen tissues were sectioned to a thickness of 5 μm and fixed with 4% paraformaldehyde (Merck). Slides were incubated with 1% BSA in PBST for 1 hour to block the non-specific antibody binding. Primary antibodies were pre-diluted in blocking buffer to 1:200 for F4/80

(CI-A3-1; Abcam) or EpCAM (G8.8; eBioscience) and applied to tissue sections overnight at 4℃ in a humidified chamber. The next day, appropriate secondary antibodies were applied, and nuclei were stained with 4,6-diamidino-2-phenylindole (DAPI; Invitrogen) before mounting. Fluorescence signals were detected using a Leica TCS SP8 confocal microscope (Leica).

Cytokine and chemokine analysis

On day 2 post-infection, the trachea of euthanized mice was exposed, transected, and intubated with a blunt 18-gage needle that delivered 0.8 mL ice-cold PBS. Infusion of the 0.5 mL volume was repeated twice, and the fluid was recovered. The recovered bronchoalveolar lavage fluid (BALF) was centrifuged at 3,000 $\times g$ for 3 minutes at 4℃ and stored at −80℃ until further use. ELISAs were performed on the BALF using TNF-α, IL-6 ELISA kits (BD Biosciences), IL-1β, CXCL1, and CXCL2 Duoset ELISA kits (R&D systems).

Cell counting

BALF was obtained via cannulation of the trachea and lavaging the airway lumen with 0.8 mL ice-cold PBS three times on day 2 post-infection. The recovered fluid was centrifuged, and the cell pellets were resuspended in PBS to count the total number of cells. Differential cell counts in the BALF were performed using the Diff-Quik staining reagent (Sysmex) according to the manufacturer's instructions. The numbers of macrophages, neutrophils, and T cells were calculated by multiplying the percentages

obtained by the total yield. Slides were imaged using the QWin program (Leica).

Histopathological scoring

Lung tissue samples were fixed in a 4% paraformaldehyde neutral buffer solution for 24 hours, dehydrated in a graded ethanol series, embedded in paraffin, sliced at 5 μm, and stained with hematoxylin and eosin. Lung histopathological score was assessed using the following parameters: a scale of 0 to 3 (0 = absent and appeared normal, 1 = light, 2 = moderate, and 3 = severe) according to the histologic features: 1) edema, hyperemia, and congestion; 2) neutrophil margination and tissue infiltration; 3) intra-alveolar hemorrhage and debris. Each parameter was scored from 0-3 based on severity. The total score was used to assess lung injury, calculated as the sum of all scores for each parameter (0-1, normal to minimal injury; 2-3, mild injury; 4-6, moderate injury; and 7-9, severe injury). The maximum score per animal was 12. Lung section scoring was performed at low power (× 40).

Quantification and statistical analysis

GraphPad Prism 8.0 (GraphPad Software) was used for the statistical analysis. Results are presented as the mean ± the standard error of the mean (SEM) for the experiments unless otherwise indicated. All between-group comparisons were carried out using analysis of variance (ANOVA) ANOVA with multiple comparisons test or Student's *t*-test. Survival data were collected from two independent experiments and are shown as

Kaplan-Meier survival curves with log-rank test. Sample size (n) is indicated in the figure legends. Statistical significance was set at P values of less than 0.05.

RESULTS

DEX/lipo is specifically delivered into the macrophages in the lungs

To deliver drugs specifically to macrophages, I encapsulated dexamethasone into liposomes with a particle size of 1,000 nm (Figure 1A). After 24 hours of intranasal injection in mice, DiI-labeled DEX/lipo was detected in the cytosol of $F4/80^+$ macrophages in the lungs (Figure 1B). I further confirmed the distribution of injected liposomes as up to 70% of DiI^+ cells were alveolar macrophages, interstitial macrophages, and monocytes (Figure 1C). In contrast, less than 10% of non-leukocytes and lymphocytes could uptake DiI^+ liposomes. In particular, up to 15.8% of monocytes, 72.5% of alveolar macrophages, and 42.2% of interstitial macrophages in the lungs were DiI^+ (Figure 1D). Gating schemes are shown in Figure 2. These results confirmed that locally delivered DEX/lipo was mainly distributed into monocytes/macrophages in the lungs.

DEX/lipo effectively reduces inflammation in mice infected with the lethal influenza virus

I determined that DEX/lipo had a therapeutic effect on mice influenza model infected with influenza A/Wisconsin/WSLH34939/09 by targeting macrophages using DEX/lipo. Mice under isoflurane anesthesia were infected intranasally with 10^5 $TCID_{50}$ of the influenza virus. One hour after infection, mice were anesthetized by isoflurane inhalation for intranasal delivery of PBS/lipo, dexamethasone (DEX), or DEX/lipo for three days.

On day 3 post-infection, mice were treated with 100 μL of PBS/lipo, DEX, or DEX/lipo intravenously. Mice were monitored for survival for 10 days. While 20% of PBS/lipo-treated mice survived on day 5 post-infection, mice treated with DEX/lipo showed the highest survival rate (40%). However, all mice treated with DEX died on day 5 (Figure 3A). Also, all mice treated with DEX rapidly lost body weight and died by day 5 post-infection. The control group (H1N1+PBS/lipo) showed significant illness as determined by loss in body weight up to 27 to 30%, whereas the DEX/lipo-treated mice showed body weight loss of 15% on day 6 post-infection. From day 7 post-infection, both the control group and H1N1+DEX/lipo group lost body weight, but H1N1+DEX/lipo group was significantly higher than the control (Figure 3B). To verify the anti-inflammatory activity of DEX/lipo on the infiltration of inflammatory cells, mice were euthanized at day 10 post-infection to obtain lung tissues for histopathological examination. In mice treated with PBS/lipo, there was a severe inflammatory response characterized by alveolar congestion, thickening of the alveolar wall, and infiltration and aggregation of immune cells in airspaces or vessel walls. However, fewer inflammatory infiltrates were observed in the lungs treated with DEX/lipo than in mice treated with PBS/lipo or DEX (Figure 3C). Consistent with these findings, the total histopathological scores also decreased significantly in the H1N1+DEX/lipo group but not in the H1N1+DEX group (Figure 3D). I also measured the virus titer to determine whether this histopathological score improvement in the H1N1+DEX/lipo group was due to the difference in

viral titers between groups. The viruses isolated from lungs plaqued on MDCK cells using $TCID_{50}$. However, the virus isolated from infected mouse lungs did not decrease in the H1N1+DEX/lipo group (Figure 3E). These results supported my hypothesis that targeting macrophages using DEX/lipo had a therapeutic effect in reducing inflammation.

DEX/lipo decreases infiltrated cells in the bronchoalveolar lavage fluid of mice with lethal influenza virus infection

To confirm DEX/lipo treatment could reduce influenza virus induced-hyper-inflammation, I analyzed the infiltrated cells in BALF collected from the lungs of mice infected with the influenza virus. Many inflammatory cells, such as monocytes, neutrophils, and lymphocytes were recruited in the lungs of mice infected with the influenza virus. The cell infiltrates in the BALF of mice treated with PBS/lipo, DEX, or DEX/lipo were statistically analyzed for cell number and type (Figure 4). DEX/lipo treatment significantly reduced the infiltration of total cells (Figures 4A and 4B). Among the infiltrating cells, not only macrophages, which are known to cause acute lung injury in the influenza virus (34), but also neutrophils and T cells were decreased in the H1N1+DEX/lipo group. Instead, DEX treatment increased the total number of infiltrated cells, especially macrophages and T cells, compared to PBS/lipo treatment (Figures 4A and 4C-E).

DEX/lipo significantly reduces the pro-inflammatory cytokines and chemokines in mice with lethal influenza virus infection

Given that inflammatory cytokines and chemokines were linked to lung damage in severe influenza pneumonia, I determined the role of DEX/lipo in mice with influenza virus infection. The protein levels of pro-inflammatory cytokines and chemokines, TNF-α, IL-1β, IL-6, CXCL1, and CXCL2 increased significantly in the H1N1+PBS/lipo and H1N1+DEX group (Figures 5A-5E). However, cytokines and chemokines were decreased dramatically in the H1N1+DEX/lipo group, except for CXCL1. (Figures 5A-5E). In particular, TNF-α and IL-1β were significantly increased in H1N1+DEX compared to the H1N1+PBS/lipo group. Furthermore, these results correlated with the infiltrated total cell number. In conclusion, my data demonstrated that the macrophage-targeting DEX/lipo played crucial roles in the prevention of pneumonia induced by the influenza virus, as well as the reduction of pro-inflammatory cytokines and chemokines and infiltration of inflammatory cells (Figure 6).

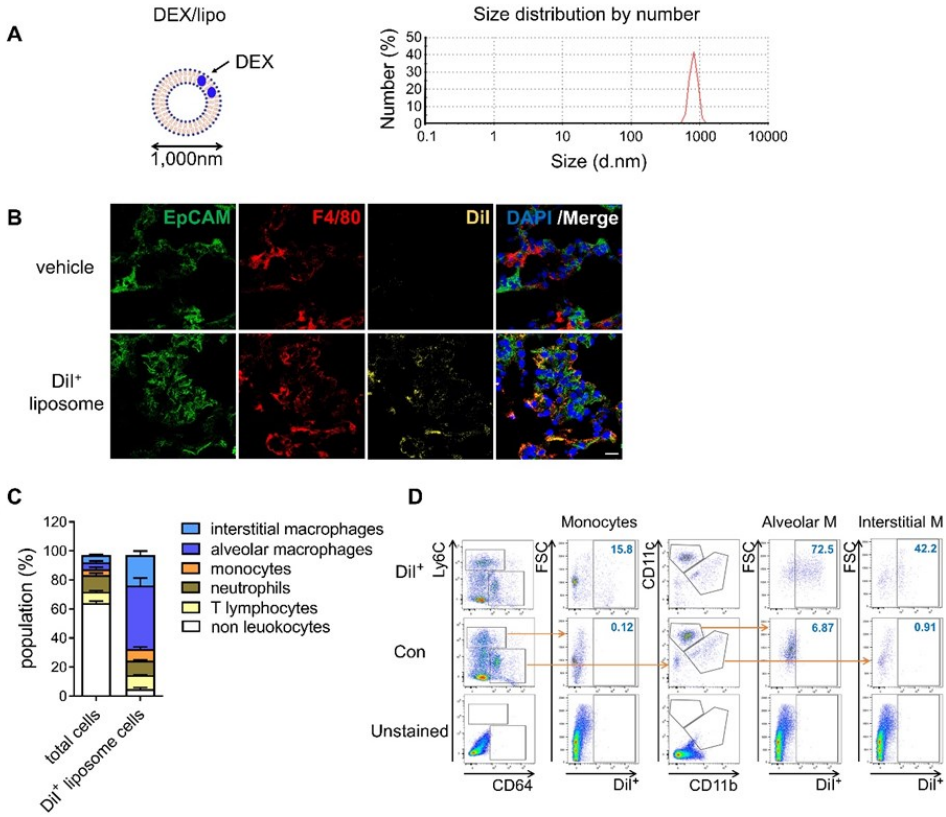

Figure 1. DEX/lipo is specifically delivered into the macrophages in the lungs. (A) Schematic of DEX/lipo, left, and size determination of DEX/lipo by dynamic light scattering (DLS), right. The mean diameter is close to 1,000 nm. **(B)** Co-immunofluorescence (Co-IF) staining was performed to confirm the co-localization of the epithelial cell adhesion molecule (EpCAM) (green) or F4/80 (red) with DiI (yellow). Mice were injected intranasally with 20 μL of DiI-labeled liposomes, and lung tissues were dissected at 24 hours post-injection. Scale bar; 20 μm. **(C)** Population percentages in the lungs of mice are shown as total cells compared to DiI^+ cells. Representatives of two independent experiments are shown. **(D)** Flow-cytometry analysis of DiI^+ cells. $CD45^+Ly6C^+CD64^{low}$ monocytes

population, $CD45^{+}Ly6C^{-}CD64^{+}CD11c^{+}$ alveolar macrophages population, and $CD45^{+}Ly6C^{-}CD64^{+}CD11b^{+}$ interstitial macrophages population are shown in the DiI/forward scatter (FSC) dot plot with gating for the DiI^{+} population.

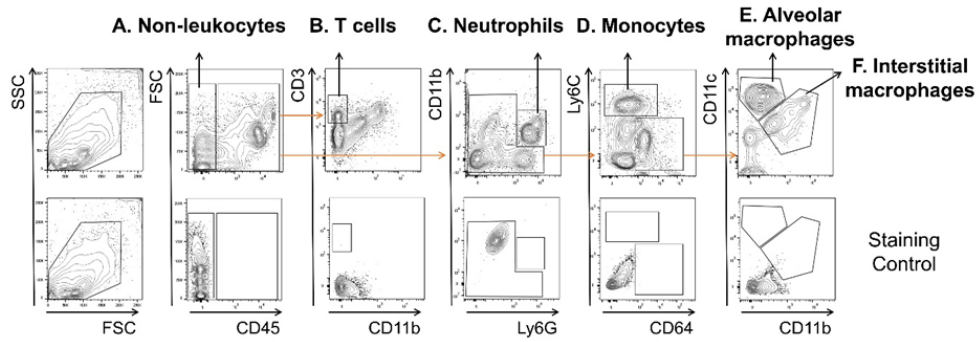

Figure 2. Gating strategies to determine the cellular compositions of the lungs of mice. Single cells were isolated from the lungs of DiI^+ injected mice and analyzed by flow cytometry. Sequentially gated cells were **(A)** $CD45^-$non−leukocytes, **(B)** $CD45^+CD11b^-CD3^+$ T cells, **(C)** $CD45^+CD11b^+Ly6G^+$ neutrophils, **(D)** $CD45^+Ly6G^-CD64^{low}$ $Ly6C^+$ monocytes, **(E)** $CD45^+Ly6G^-CD64^+CD11c^+$ alveolar macrophages, **(F)** $CD45^+Ly6G^-CD64^+CD11b^+$ interstitial macrophages. Representative dot plots are shown.

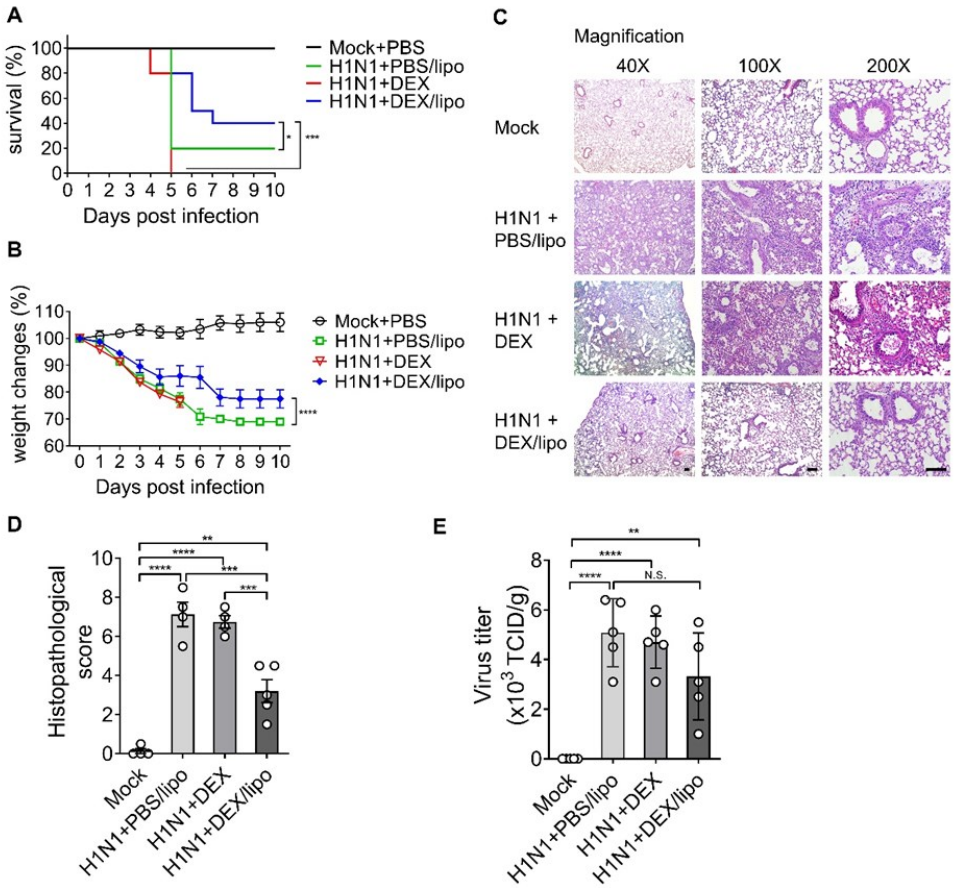

Figure 3. DEX/lipo effectively reduces inflammation in mice infected with the lethal influenza A virus. Mice were infected intranasally with 10^5 $TCID_{50}$ of the influenza virus and treated with PBS/lipo, DEX, or DEX/lipo. Mice were monitored daily to record survival rates and body weight changes. **(A)** Survival rate of infected mice (n = 10 per group) after PBS/lipo, DEX, or DEX/lipo treatment. $*P < 0.05$, $***P < 0.001$ by Kaplan–Meier survival curves with log–rank test. Data were collected from two independent experiments. **(B)** Body weight change of infected mice (n = 10 per group) after PBS/lipo, DEX, or DEX/lipo treatment. $***P < 0.001$ by the two–way ANOVA with multiple comparisons test. **(C)** Hematoxylin and

eosin staining of the lungs on day 10 post-infection. (n = 5 per group) Scale bar; 100 μm. **(D)** Comparison of the total histopathological scores of lung injury. (n = 4-5 per group) Data are presented as the mean ± SEM. $^{**}P < 0.005$, $^{***}P < 0.001$, $^{****}P < 0.0001$ by the one-way ANOVA with multiple comparisons test. **(E)** Lung viral titers from mice on day 10 post-infection using $TCID_{50}$ (n = 4-5 per group). Data are presented as the mean ± SEM. $^{**}P < 0.01$, $^{****}P < 0.0001$ in the one-way ANOVA with multiple comparisons test.

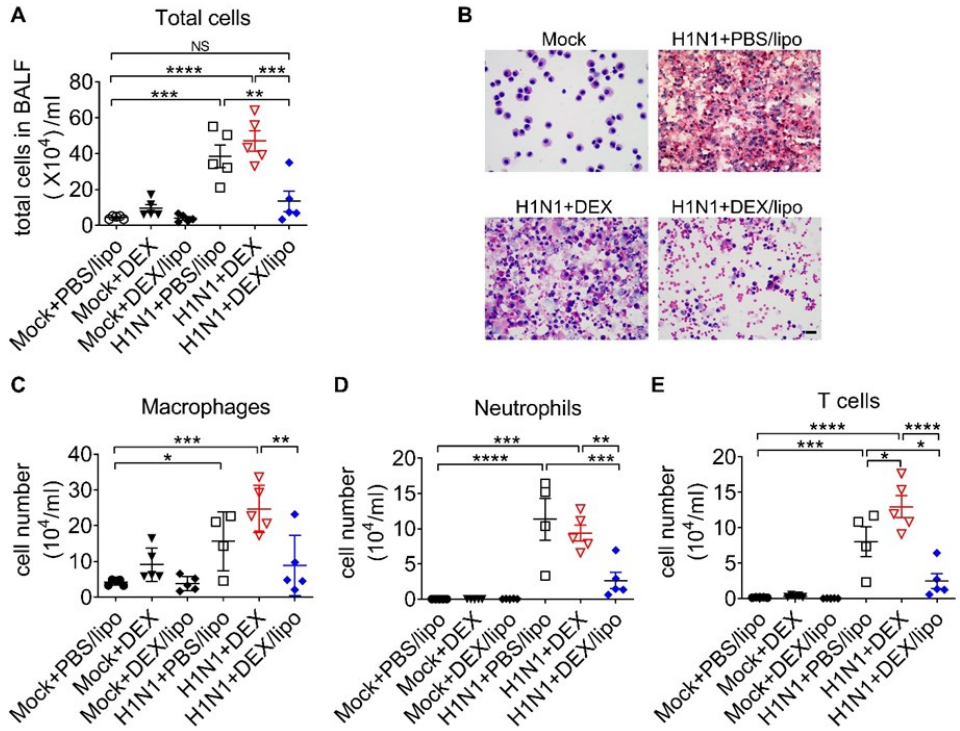

Figure 4. DEX/lipo decreases the total number of cells in the bronchoalveolar lavage fluid of mice with lethal influenza virus infection. (A) Analysis of the total number of infiltrated cells in the BALF collected from the mock or influenza virus-infected mice treated with PBS/lipo, DEX, or DEX/lipo (n = 4-5 per group) on day 2 post-infection **(B)**. Differential cell counts of BALF cells. Representative pictures of Diff-quick staining of cytospin preparation. Scale bar; 20 μm Changes in the number of macrophages **(C)**, neutrophils **(D)**, and T cells **(E)**. BALF cells were counted using the QWin program (Leica Microsystems). Data are presented as the mean ± SEM and represent two independent experiments. *P < 0.05, **P < 0.01, ***P < 0.001, ****P < 0.0001 by the one-way ANOVA test with multiple comparisons test.

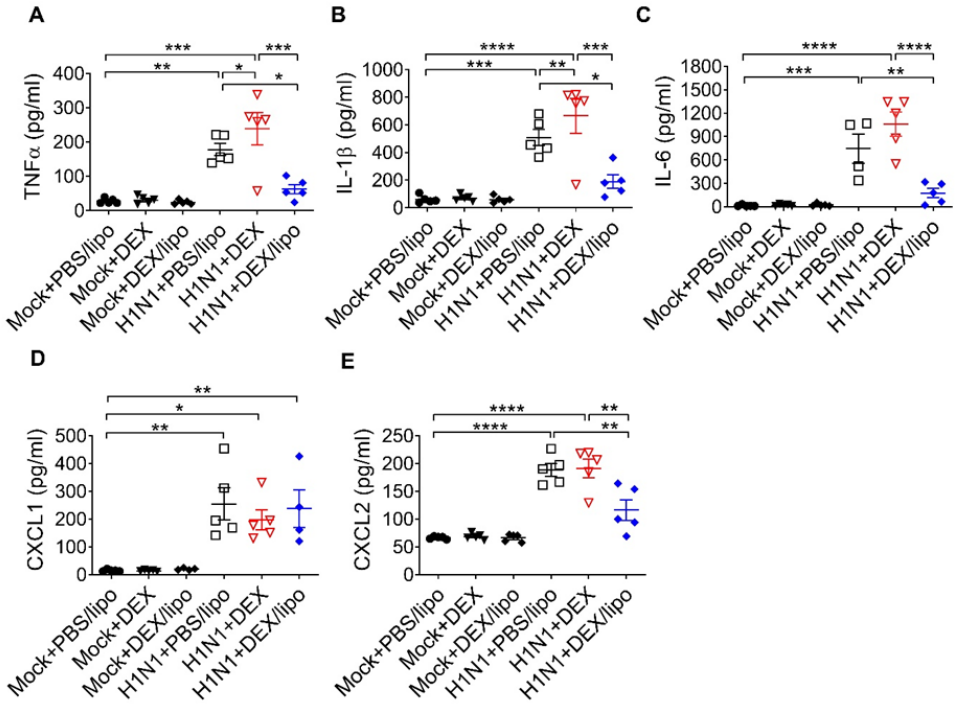

Figure 5. DEX/lipo significantly reduces the pro-inflammatory cytokines and chemokines in mice with lethal influenza virus infection (A-E). Analysis of the inflammatory cytokines and chemokines collected from BALF of mock or influenza virus-infected mice treated with PBS/lipo, DEX, or DEX/lipo (n = 4-5 per group) on day 2 post-infection. TNF-α **(A)**, IL-1β **(B)**, IL-6 **(C)**, CXCL-1 **(D)**, and CXCL2 **(E)** were measured by the ELISA. Data are presented as the means ± SEM and represent two independent experiments. *P < 0.05, **P < 0.01, ***P < 0.001, ****P < 0.0001 by the one-way ANOVA with multiple comparisons test.

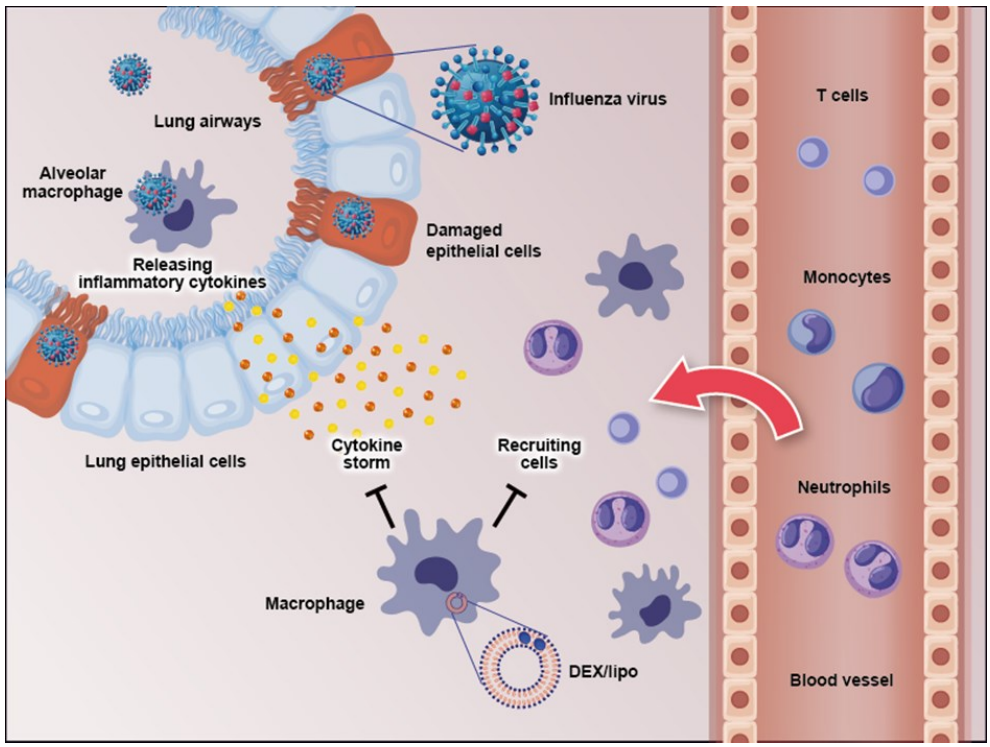

Figure 6. Schematic figure of the effects of DEX/lipo on the pathogenesis of the influenza virus infection. Influenza virus infects the lung epithelial cells and, subsequently, alveolar macrophages. As a result, inflammatory macrophages secrete pro-inflammatory cytokines and chemokines. In addition, specific pro-inflammatory cytokines lead to the recruitment of neutrophils, monocytes, macrophages, and T cells into the site of infection. DEX/lipo delivery targeting macrophages reduces cytokines/chemokines secretion and recruitment of leukocytes to the lung of mice with lethal influenza virus infection.

Discussions

This study aimed to alleviate hyper-inflammation in the lungs caused by lethal influenza virus infection by delivering DEX/lipo, specially targeting macrophages. To achieve this goal, I manufactured liposomes with a large size (1,000 nm) that could be loaded with anti-inflammatory drugs and evaluated their size by DLS. Because many other studies showed that liposomes with relatively larger diameters were more effectively distributed into phagocytes (22, 47, 48). Also, I found the made liposome are distributed in $F4/80^+$ macrophages in lungs by immunofluorescence; $CD45^+Ly6G^-CD64^+CD11c^+$ alveolar macrophages and $CD45^+Ly6G^-CD64^+CD11b^+$ interstitial macrophages by FACS. Although I could not specifically separate dendritic cells from macrophages with markers such as MHC class II and CX3CR1, Samira T *et al.* reported that $CD11c^{hi}CD64^-$ and $CD11c^{-to\ int}CD64^+$ subsets distinguished macrophages from dendritic cells using CCR2 deficiency mice (49). Therefore, my data showed that 1,000 nm-sized liposomes could target macrophages.

Meanwhile, I revealed that DEX/lipo effectively reduced pro-inflammatory responses in mice with pathogenic A/H1N1 influenza virus infection, demonstrating the possible availability of DEX/lipo in controlling hyper-inflammation in respiratory diseases. In addition, I used the mouse-adapted influenza virus to mimic human influenza pathogenesis. Pathogenesis in human influenza virus infection is accompanied by diffuse epithelial sloughing in tracheal, bronchial, and bronchiole biopsy, the

predominant presence of mononuclear cells, and bloody exudate in the airway lumen with interstitial swelling (50, 51). In line with this, the mice model of human pathogenic pandemic A/Wisconsin/*WSLH34939/09* influenza virus infection showed 80% of death within 12 days post-infection with significant tissue injury, including hemorrhage, pulmonary edema and mononuclear cell accumulation (52). Furthermore, the mouse-adapted influenza virus infection model showed the same characteristic histopathological findings, including alveolar congestion and infiltration of macrophages in airway spaces, showing comparable results (Figures 3 and 4). Of note, cytokines, such as TNF-α and IL-6, all of which are known to be directly correlated with host morbidity and pulmonary injury (53-55), were significantly elevated in bronchoalveolar lavage fluids on day 2 post-infection (Figures 5A and 5C), implying the importance of immune responses in the disease pathogenesis of my influenza virus infection model.

There were several significant findings to be discussed. First, the most notable results in this study were the differences in the therapeutic responses of DEX/lipo compared to the free dexamethasone. Intranasal delivery of free dexamethasone did not alleviate tissue injury in the infected mice (Figure 3C). I thought that the encapsulation of dexamethasone into liposomes enhanced efficacy and reduced toxicity as the compared same amount of free dexamethasone. Also, there was a previous report that glucocorticoid encapsulation reduced the migration of monocytes and macrophages by regulating chemokines such as MCP-1

(56). Second, DEX/lipo could be delivered specifically to macrophages, whereas DEX could be delivered to other cells, such as lung epithelial cells. Based on the previous study that corticosteroids induced apoptosis of airway epithelial cells (57), it could be speculated that DEX treatment induced robust damages such as epithelial cell death resulting in more severe inflammatory responses in the lungs. In my study, I treated DEX immediately within one hour after the influenza virus infection. If DEX treatment is delayed by 24−48 hours after influenza virus infection, it is difficult to suppress the initial excessive inflammatory responses, even though most DEX treatments will be delivered after symptom onset. This was further supported by the results shown in Figures 4 and 5, because free dexamethasone did not block the accumulation of macrophages and T cells or decrease TNF−α, IL−1β, IL−6, and CXCL2 in BALF. Free dexamethasone accelerated the fatality rate of infected mice from 80% to 100% (Figure 3B), possibly due to increased T cells, TNF−α, and IL−1β in airway spaces.

In contrast, DEX/lipo treatment rescued infected mice from death compared to free dexamethasone, with a significant decrease in tissue damage, infiltration of macrophages and T cells, and accumulation of TNF−α, IL−1β, IL−6, and CXCL2 in the lungs. These results were consistent with concerns from previous observations of dexamethasone toxicities in the clinic (57−59). Further, I demonstrated the usability of liposomes as delivery cargo in improving the safety and effectiveness of dexamethasone in controlling influenza virus infection.

There have been many cases in which DEX/lipo, mainly targeting macrophages, was delivered to reduce inflammation in various diseases. Polyethylene glycol (PEG)-free formulation of macrophage-targeting DEX/lipo reduced the dose and frequency required to treat adjuvant arthritis, with the potential to enhance or prolong therapeutic efficacy and limit side effects in the treatment of rheumatoid arthritis (60). Additionally, the administration of tumor-associated macrophage (TAM)-targeting DEX/lipo resulted in significant inhibition of tumor growth and metastasis in a model of prostate cancer bone metastases (61). In particular, macrophages were known as an essential producer of inflammatory cytokines in influenza virus infection, and I showed that DEX/lipo was effectively distributed into monocytes/macrophages (Figure 3C). The fact that DEX/lipo did not reduce CXCL1, produced mainly by epithelial cells and not by macrophages (Figure 5D), further supported our hypothesis that liposomal encapsulation specifically delivered dexamethasone into macrophages but not epithelial cells.

An immunomodulatory agent should accompany antiviral therapy because antiviral drugs do not directly inhibit inflammation in pulmonary injury. In my study, even the single treatment of DEX/lipo decreased inflammatory cytokines and increased the survival rate.

In conclusion, my data demonstrated that the macrophage-targeting DEX/lipo played crucial roles in the prevention of pneumonia induced by the influenza virus, as well as the reduction of pro-inflammatory cytokines and chemokines and infiltration of inflammatory cells (Figure 6).

Therefore, targeting macrophages using DEX/lipo may be a promising therapeutic approach for treating hyper-inflammation-induced lethal doses of influenza virus infection with antiviral drugs.

CHAPTER 2

Severe Dengue virus Infection-mediated Suppression of IL-12 Reduces Antiviral Response by CLEC5A and FcγR signaling in Macrophages

INTRODUCTION

Dengue virus (DV) is a mosquito-borne infection caused by four serotypes of dengue virus (DV1-DV4) and is currently the most common arthropod-borne disease in tropical and subtropical areas (62-64). Even though most patients infected by DV are asymptomatic, DV infection can cause a broad spectrum of clinical symptoms, ranging from dengue fever (DF), an acute, self-limited febrile illness, to the life-threatening dengue hemorrhagic fever and dengue shock syndrome (DHF/DSS), characterized by plasma leakage, low platelet counts, liver damage, elevated cytokine levels, and, in the most severe cases, death due to shock (62, 65). However, the pathogenesis of the DHF/DSS remains unclear, but massive cytokine secretion is believed to be one of the significant contributory factors (66-68). In contrast to other inflammatory cytokines, IL-12 was decreased in the plasma of DHF/DSS patients compared to DF patients (25, 31). However, whether the decrease in IL-12 causes the DHF/DSS has not been determined.

IL-12 is an inflammatory cytokine comprised of p35 and p40 subunits (69). It is secreted by macrophages and antigen-presenting cells (APCs) and is involved in the early stages of immune response (70). IL-12 stimulates the secretion of several cytokines, in particular IFN-γ, by both T and natural killer cells (NK cells) (71, 72). IL-12 has been recently demonstrated to be a component of the complex signal network between leukocytes and neoplastic cells. The early effect of IL-12 on tumor

behavior is the inhibition of angiogenesis, resulting in ischemic necrosis (73-75). Also, MMP-9 can be a molecular target of IL-12-dependent cross-talk between immune and vascular cells (76). Based on these results, I hypothesized that IL-12, which was specifically reduced by severe DV infection, increased MMP-9, resulting in DHF.

Monocytes and macrophages are the primary sources of inflammatory cytokines and the central target cells for DV replication (77, 78). DV binds human mannose receptor (MR) and dendritic cell-specific intercellular adhesion molecule-3-grabbing non-integrin (DC-SIGN) on macrophages as primary receptors and CLEC5A as a signaling receptor to sense the DV invasion and then to signal and stimulate macrophages to secrete pro-inflammatory cytokines (79). Also, CLEC5A is critical to regulate NLR family pyrin domain containing 3 (NLRP3) inflammasome activation in DV infection, and CLEC5A can cause clinical symptoms in DHF/DSS (80). Meanwhile, the other cause of DHF/DSS is known as an ADE of infection in which sub-neutralizing levels of DV-specific antibodies exacerbate disease by increasing infection of cells bearing FcγRs (81, 82). However, little is known about the mechanism of this receptor-mediated IL-12 decrease and its contribution to pathology, such as increased disease severity due to MMP-9 on vascular permeability.

Therefore, I investigate the mechanism of human macrophage signaling events involved in the production of IL-12. Here, I identify CLEC5A and FcγR as suppressors of IL-12. It is known that IRF1 is

crucial for IL-12 production by inducing nucleosome remodeling of *IL12A*. This study demonstrates that severe DV infection (e.g., high doses of DV infection or ADE of DV infection) triggers CLEC5A or FcγR, which leads to specific degradation of IRF1, thereby suppressing *IL12A* transcription in macrophages. CLEC5A and FcγR signaling lead to E3 ubiquitin ligase MDM2-dependent proteasomal degradation of IRF1 in the nucleus. Furthermore, I report that high doses of DV infection and ADE of DV infection induce vascular permeability *in vitro* and *in vivo* by down-regulating IL-12 production to induce MMP-9. These observations suggest that IL-12 is critical for regulating vascular permeability in severe DV infection and that the blockade of IL-12 suppressor can be helpful to alleviate clinical symptoms in DHF/DSS patients.

MATERIALS AND METHODS

Animals

Male or female type I interferon receptor knockout (IFNAR KO) mice gifted by Jo' s Lab (Seoul National University). Animal experiments were conducted at the Institute for Experimental Animals, College of Medicine and cared for according to the Guide for the Care and Use of Laboratory. The study was approved by the Seoul National University Animal Care and Use Committee (accession number SNU-210909-5-1). Mice were housed in cages with constant-flow air exchange, supporting specific pathogen-free conditions.

Amplification of Dengue virus

Dengue virus type 2 (DV2, NCCP No. 43255) was obtained from the National Culture Collection for Pathogens (NCCP). DV2 was propagated in the kidney of an African green monkey cell line Vero E6 (clone E6; American Type Culture Collection) for 5 days. Virus titers were obtained by focus-forming unit assay on Vero E6 cells. The DV2 stock was 10-fold serially diluted, and each dilution was inoculated onto Vero E6 cell monolayers in 96-well culture plates in duplicate. Virus inoculums were allowed to absorb onto the cell monolayers for 1 hour at 37℃ before discarding. The culture plates were overlaid with a semisolid media containing 1×opti-MEM, 2% FBS, and 1% carboxymethyl cellulose. The culture plates were fixed and permeabilized on 2 day post-infection with

cold methanol. The plates were then stained with an E60 monoclonal antibody followed by a goat anti-mouse IgG conjugated antibody with horseradish peroxidase (Invitrogen). Finally, the chromogenic substrate 3, 3'-diaminobenzidine tetrahydrochloride (DAB), was added, producing dark brown foci in antigen-positive cells. The viral titers were presented as foci-forming units (FFUs)/mL. For a high dose of DV infection, the virus was concentrated by centrifugation at 100,000 $\times g$ for 4 hours at 4℃ and re-suspended in cold PBS.

Cell line culture and monoclonal antibodies

The cell lines, including Vero E6 and THP-1, were cultured in RPMI 1640 or DMEM with 10% FBS and 1% PS. Human umbilical vein endothelial cells (HUVECs) were cultured in the EGM-BulletKit medium (Lonza). All cells were cultured at 37℃ and 5% CO_2 in a humidified incubator. THP-1 cells were differentiated into macrophages by 24 hours incubation with 100 ng/mL of phorbol 12-myristate 13-acetate (PMA) (Sigma-Aldrich) followed by 24 hours incubation in RPMI medium. Macrophages were polarized in M1 macrophages by incubation with 30 ng/mL of PMA, 20 ng/mL of human IFN-γ (peprotech), and 20 ng/mL of LPS (Sigma-Aldrich) for 48 hours incubation in RPMI medium. Macrophages were polarized in M2 macrophages by incubation with 30 ng/mL of PMA and 20 ng/mL of human IL-4 (peprotech) for 48 hours of incubation in RPMI medium. For some experiments, macrophages are treated with 10, 100, and 1,000 ng/mL human recombinant IL-12 (peprotech). For investigation

of DV binding FcγR signaling, human E60-IgG1 (hE60) and hE60-N297Q (N297Q) were obtained from S. Johnson (MacroGenics Inc.). The mouse E60 IgG2a mAb was originally generated against WNV E protein, reacts with an epitope in the fusion peptide in domain II, and cross-reacts with DV E proteins (83). The generation of a chimeric human-mouse E60 with the human IgG1 constant regions and the mouse VH and VL was performed as described previously (84). Point mutations in the Fc region that abolish FcγR (N297Q) were introduced by QuikChange mutagenesis (Stratagene).

DV2 Infection to THP-1

THP-1 cells were seeded in a cell culture plate (CORNING) at 6×10^5 cells/mL and differentiated into inflammatory macrophages for 3 days, as described above. After polarization of inflammatory macrophages, DV2 diluted in a culture medium was added to each well at the final multiplicity of infection (MOI) of 1 or 30. For ADE of DV infection, 1 μg/mL of DV3 antibody (5D4-11; Sigma-Aldrich), or 0.1 μg/mL of hE60, or 0.1 μg/mL of hE60-N297Q were performed with DV2 (1 MOI) during 1 hour at 37℃. Then, cells were incubated with virus/antibody complexes for 1 hour at 37℃ with 5% CO_2 to ensure virus adsorption. Cells were washed twice with PBS and cultured in fresh medium supplemented with 2% FBS before they were harvested at each time point.

Infection with DV2 in IFNAR KO mice

Mice were injected intraperitoneally with PBS, or anti-DV3 antibody, in a total volume of 200 μL, then infected 24 hours later with 10^5 or 10^7 FFU

of DV2 by iv injection into the tail vein in a total volume of 100 μL. In addition, some mice were treated with 50 μg/kg of recombinant IL-12 (peprotech) or 1 mg/kg of Nutlin-3A (Sigma-Aldrich), known as MDM2 inhibitor on 1 hour post-infection and day 2 post-infection twice. On day 5 post-infection, mice were fully anesthetized with ketamine/xylazine, and plasma was collected through the cardiac puncture to titrate viral RNA and measure cytokines. Infected mice tissues were harvested for further analysis. Also, the mice were monitored for body weight and survival for 10 days.

RNA Extraction and Real-time PCR

RNA was solubilized in RNAiso reagent (Takara) and extracted according to the manufacturer's instructions. cDNA was synthesized from 1 μg total RNA, and the mRNA levels were determined by quantitative real-time PCR using the Reverse Transcription kits (Enzynomics). Gene expression was determined by quantitative real-time PCR using SYBR Green (Enzynomics) on a Bio-rad PCR system. The relative amount of each mRNA was normalized by *RPL37A* expression. Sequences of primers used for amplification were as follows: IL-12p35 forward, 5'-AGG CCC TGA ATT TCA ACA-3'; reverse, 5'-GAT GTA ATA GTC CCA TCC TTC TTT-3'; IL-12p40 forward, 5'-GCT ATG GTG AGC CGT GAT-3'; reverse, 5'-CAT GCT AAT GAG AAA GGG ATT-3'; *RPL37A* forward, 5'-ATT GAA ATC AGC CAG CAC GC-3'; reverse, 5'-AGG AAC CAC AGT GCC AGA TCC-3'.

Permeability assay

HUVECs were seeded at 3×10^5 cells/well on matrigel (CORNING)-coated 0.4 μm pore size filters in the transwell (CORNING) inserts using EBM-2 medium with an EGM-2 bullet kit containing 2% FBS, antibiotics, and a mixture of growth factors according to the supplier's instructions (LONZA) at 37℃ under humidified 5% CO_2 for 3 days. 24 hours after treatment with Mock, DV2 1MOI, DV2 30 MOI, DV2-αDV3, DV2-E60, or DV2-N297Q of THP-1 infected supernatant, and 70 kDa FITC-conjugated dextran (Sigma-Aldrich) was administered to the upper compartments of the inserts. 10 minutes after adding dextran, the fluorescence intensity of the medium in the lower compartments was measured by the fluorescent microplate reader (Tecan) at an excitation of 490 nm and an emission of 538 nm.

Gel zymography

MMP-9 activity was measured by zymography assay on THP-1 supernatants. Briefly, cell supernatants were collected and centrifuged at 500 $\times g$ for 5 minutes at 4℃. Ten micrograms of proteins were separated by 10% SDS-PAGE impregnated with 4 mg/mL of gelatin (Sigma-Aldrich) in non-reducing conditions. Gels were washed twice for 20 minutes with 50 mM Tris and 2.5% Triton X-100 (pH 7.5) and incubated overnight at 37℃ in 40 mM Tris, 200 mM NaCl, 10 mM $CaCl_2$, and 0.02% NaN_3 (pH 7.5) with 5 mM EDTA. Clear bands were visualized on the blue

background after staining with 0.25% Coomassie blue R250 and destained with 50% methanol and 10% acetic acid. Densitometric analysis of the bands was performed with Gel Doc XR System (bio rad).

Viral RNA isolation and Quantification

Viral RNA was isolated from the supernatant of THP-1 infected with DV2 or the plasma of mice infected with DV2 using a viral isolation kit (Bioneer). cDNA synthesis and PCR amplification with the SYBR Green method were performed as described above. Sequences of primers used for amplification were as follows: DV2 forward, 5'-AGA AAG AGG GAG GAG CAA TGT ATG-3'; reverse, 5'-TTT AGG TCT TCT AGT GTG ATT CTT GTA TCC-3'.

Western blotting

To obtain total cell lysates, cells were lysed in RIPA buffer (LPS Soultion) with protease inhibitor (gendepot) and phosphatase inhibitor (gendepot). The total cell lysates were sonicated for 30 seconds and heated to 100℃ for 5 minutes. Separately to obtain nuclear and cytoplasmic proteins, the cells were re-suspended in 500 μL 1×hypotonic buffer by pipetting up and down several times and incubated on ice for 15 minutes. After incubation, add 50 μL of 10% triton X-100 and vortex for 10 seconds at the highest setting. And centrifuge the homogenate for 10 minutes at 1,000 ×g at 4℃ and transfer and save the supernatant (cytoplasmic proteins, CE). The remained pellet was re-suspended in 50 μL Complete

Cell Extraction Buffer (Invitrogen) for 30 minutes on ice. Finally, centrifuge for 10 minutes at 14,000 $\times g$ at 4℃ and transfer supernatant (nuclear proteins, NE) to a clean tube. Each obtained protein was determined by BCA protein assay. To obtain tissue lysates, lungs from infected mice were homogenized by Tissue LyserII (QIAGEN). Protein samples were separated on 8~12% SDS-PAGE. After electrophoresis, proteins were transferred to nitrocellulose membrane (Millipore) and then washed with PBS containing 0.05% Tween-20 (PBST) and then blocked with PBS containing 5% skim milk or 5% BSA for 1 hour at room temperature. Membranes were then probed with anti-phospho-PI3K (Cell Signaling Technology), anti-PI3K (19H8; Cell Signaling Technology), anti-phospho-Akt (Cell Signaling Technology), anti-Akt (Cell Signaling Technology), anti-phospho-MDM2 (Invitrogen), anti-MDM2 (IF2; Invitrogen), anti-IRF-1 (D5E4; Cell Signaling Technology), anti-Rpb1 CTD (4H8; Cell Signaling Technology), anti-ZO-1 (Invitrogen), anti-E-cadherin (24E10; Cell Signaling Technology), anti-N-cadherin (H-63; Santa Cruz Biotechnology), or anti-β-actin (C4; Santa Cruz Biotechnology) antibodies at 1/3,000 overnight. After washing three times, blots were incubated with HRP-conjugated appropriate secondary antibodies (Santa Cruz Biotechnology) at 1/5,000 for 2 hours at room temperature. Immunoreactivity was detected using the Femto Lucent detection kit (Invitrogen).

RNA interference

THP-1 derived macrophages transfected with 25 nM siRNA using Lipofectamine™ RNAiMAX Transfection Reagent (Invitrogen). siRNAs used were: CLEC5A (SR308396), CARD9 (SR324849), BCL10 (SR305897), MALT1 (SR307428), IRF1 (SR302445), MDM2 (SR320944) and non-targeting siRNA (SR30004) as a control (Origene). Silencing of expression was verified by real-time PCR after 48 hours of transfection.

Chromatin Immunoprecipitation Assay

Chromatin immunoprecipitation (ChIP) assays were performed using manual instruction. Briefly, THP-1 cells were fixed with 1% (vol/vol) paraformaldehyde after 24 hours of infection, nuclei were isolated, and chromatin DNA was fragmented by sonication. Protein-DNA complexes were immunoprecipitated using anti-p65 (D14E12; Cell Signaling Technology), anti-Rpb1 CTD (4H8; Cell Signaling Technology), anti-IRF1 (D5E4; Cell Signaling Technology) antibodies or negative control IgG (Invitrogen), and coated on protein G PLUS agarose beads (Santa Cruz Biotechnology). DNA was purified after the reversal of crosslinks. Real-time PCR reactions were performed with primer sets spanning the TATA box, NF-κB, and ISRE binding sites. To normalize for DNA input, a sample for each condition was taken that had not undergone immunoprecipitation (input DNA); results are expressed as percent input DNA.

NF-κB DNA binding assay

Nuclear extracts of THP-1 were prepared after 24 hours of DV2 infection using the manual protocol as described above. NF-κB DNA binding was determined using the TransAM NF-κB family kit (Active Motif).

Chromatin Accessibility Real-Time PCR Assay

Chromatin accessibility real-time (ChART) assays were performed to measure *IL12A* nucleosome remodeling. Briefly, nuclei were isolated after 24 hours of DV2 infection, digested with *Bst*XI or EcoRI, and DNA was purified. Real-time PCR reactions were performed with primer sets spanning (A) the *Bst*XI site located at nt −298 that becomes available after nuc-2 remodeling, (B) the *Bst*XI site located at nt 456 that is not subject to chromatin alterations as an internal control, and (C) GAPDH to normalize for DNA input. Results are expressed as percent remodeling observed in the EcoRI-digested sample for each cell treatment using the formula $(Nt_{EcoRI} - {}_{BstXI})/Nt_{EcoRI}$ x 100%, with $Nt = 2^{Ct(C)-Ct(A)}$.

Cellular Localization and Association of MDM2 and IRF1

Nuclear and cytoplasmic extracts of THP-1 were prepared after 24 hours of DV2, as described above. For detection of the association between MDM2 and IRF1, extracts were prepared from THP-1 stimulated in the presence of 100 nM proteasome inhibitor MG-132 (calbiochem). MDM2-IRF1 complexes were immunoprecipitated from 20 mg of the nuclear extract with anti-IRF1 (D5E4; Cell Signaling Technology) antibody coated on protein G PLUS agarose beads (Santa Cruz Biotechnology). Proteins

were resolved by SDS-PAGE, and MDM2 and IRF1 were detected by immunoblotting.

Immunofluorescence (IF)

IRF1 localization was further determined by immunofluorescence staining; THP-1 was infected DV2, fixed with 1% paraformaldehyde, then permeabilized with 0.2% (vol/vol) Triton X-100 in PBS, and stained with anti-IRF1 antibody. Incubation of Alexa Fluor 594-conjugated anti-rabbit antibody (Invitrogen) was followed by staining of nuclei with DAPI (Invitrogen). IRF1 localization was visualized with a Leica TCS SP8 confocal microscope (Leica).

Cytokine and Chemokine Analyses

Cell culture supernatants were harvested after 48 hours of DV2 infection, and concentrations of TNF-α, IL-6, IL-12p70, IL-12p40, and TIMP-1 were determined by ELISA (R&D systems). The plasma obtained from mice infected with DV2 was centrifuged at 3,000 $\times g$ for 3 minutes at 4℃ and stored at −80℃ until further use. ELISAs were performed on the plasma using sample kits as described above.

Quantification and statistical analysis

GraphPad Prism 8.0 (GraphPad Software) was used for the statistical analysis. Results are presented as the mean ± SEM for the experiments unless otherwise indicated. All between-group comparisons were carried out using ANOVA with multiple comparisons test or Student's *t*-test.

Survival data were collected from two independent experiments and are shown as Kaplan–Meier survival curves with log–rank test. Sample size (n) is indicated in the figure legends. Statistical significance was set at P values of less than 0.05.

RESULTS

In vitro modeling of severe DV2 infection in M1 type of THP-1

To establish the *in vitro* model of severe DV2, I examined the mRNA level of *FCGR1A*, *FCGR2A*, *FCGR2B*, *CD206*, *CD209*, and *CLEC5A* in different types of THP-1-derived macrophages (Figure 7A). As expected, the level of *FCGR2A* mRNA, which activates immunoreceptor tyrosine-based activation motif (ITAM) signaling, was increased in the M1 macrophage type, and the level of *FCGR2B* mRNA, which activates Immunoreceptor tyrosine-based inhibitory motif (ITIM) signaling, was increased in M2 type. Among the receptors, the C-type lectin receptors *CD206*, *CD209*, and *CLEC5A* have previously been shown to interact with glycans located on the envelope (E) protein of DV (80, 85). After confirming that the level of *FCGR2A* and *CLEC5A* mRNA was increased in inflammatory macrophages, I established severe DV infection conditions according to several conditions in inflammatory macrophages. Severe DV conditions that increase vascular permeability include 1) high dose of DV infection (30 MOI of DV2), 2) ADE of DV infection (DV2-αDV3, DV2-E60). In addition, an E60-N297Q antibody that could not bind to FcγR was used as a negative control of FcγR signaling (description of the antibodies is described in the Method and Material section). After infection with inflammatory macrophages according to each viral infection condition, viral RNA was quantified in the cell culture supernatant after 48 hours. I confirmed that viral RNA was increased in the 30 MOI of DV2 infection group and ADE of DV infection group (DV2-αDV3, DV2-E60) than in the

1 MOI of DV2 infection group. The DV2-N297Q group also increased compared to the 1 MOI of DV2 infection group but decreased significantly compared to the DV2-E60 group (Figure 7B). These results showed that FCγR signaling was involved in severe DV infection. Also, my results did not conflict with previous studies that inflammatory macrophages caused DHF/DSS by secreting pro-inflammatory cytokines through CLEC5A signaling (80, 86); I established *in vitro* model of severe DV through inflammatory macrophages in my study.

Treatment of recombinant IL-12 inhibits vascular permeability and MMP-9 activity.

Unlike other pro-inflammatory cytokines, only IL-12 was specifically decreased in the serum of DHF/DSS patients (31). Therefore, I wondered whether IL-12 might participate in the pathogenesis of DHF/DSS. Since the M1 type of THP-1 cells secreted many inflammatory cytokines, I collected the cell culture supernatants in the presence or absence of recombinant IL-12 treatment for 72 hours. HUVEC permeability was measured in THP-1 M1 supernatant for 24 hours using transwell assay (Figure 8A). Interestingly, the THP-1 M1 supernatant treated with recombinant IL-12 had reduced HUVEC permeability (Figure 8B). After that, I treated a gradient manner of recombinant IL-12 (0-1,000 ng/mL) in the M1 type of THP-1 and confirmed the activity of MMP-9 in each treated group through a zymography assay. I found that the activity of MMP-9 was reduced in the highest concentration of recombinant IL-12

(Figure 8C). These results suggest that IL-12 alone modulates vascular permeability by regulating MMP-9.

Treatment of recombinant IL-12 increases the pro-inflammatory cytokines and TIMP-1 in THP-1 infected with severe DV2

The permeability of HUVECs was decreased in the THP-1 M1 treated with recombinant IL-12 group. However, I thought several cytokines could affect endothelial permeability. Therefore, to confirm whether this is the effect of recombinant IL-12, TNF-α and IL-6 were measured in the supernatant treated with or without IL-12 after infection of severe DV2. TNF-α and IL-6 were increased in the high dose of DV2 and ADE infection of DV2 (Figures 9A and B). However, IL-12p70 was decreased in the high dose of DV2 and ADE infection of DV2 as in the DHF/DSS patients (Figure 9C). I also found that TNF-α, IL-6, IL-12p70, and TIMP-1, known as the inhibitory regulator of MMP-9, were increased in the supernatant treated with recombinant IL-12 (Figures 9A-D). Since inflammatory cytokines such as TNF-α are known to increase vascular permeability, I thought IL-12 could regulate TIMP-1-mediated vascular permeability independent of inflammatory cytokines.

Treatment of recombinant IL-12 significantly inhibits dengue hemorrhagic fever in mice with a severe infection of DV2.

Next, I established the *in vivo* severe DV2 infection model that causes DHF to confirm the effect of recombinant IL-12 in IFNAR KO mice

(detailed methods are described above). Elevated levels of various cytokines (TNF-α, IL-6, IL-10, and IL-8), increased vascular permeability, thrombocytopenia, increased hematocrit, and gastrointestinal bleeding are hallmarks of DHF/DSS in humans. Therefore, I validated the effect of recombinant IL-12 as DHF treatment in IFNAR KO-infected mice through the above indicators. For 5 days after infection, the body weight of the mice was decreased in the DV2-αDV3 group more than in the DV2 group, and it was recovered in the DV2-αDV3 group treated with recombinant IL-12 (Figure 10A). I confirmed that the viral RNA isolated from mouse plasma was significantly higher in the DV2-αDV3 group than in the DV2 group and decreased in the DV2-αDV3 group treated with recombinant IL-12 (Figure 10B). I thought the early recombinant IL-12 treatment might help kill the virus by activating the Th1 response. I also measured cytokines in mouse plasma by ELISA. As with the previous *in vitro* results, TNF-α and IL-6 were increased in the DV2-αDV3 group and were decreased in the DV2-αDV3 group treated with recombinant IL-12. IL-10 had no effect, and IL-12p70 was reduced in the DV2-α DV3 group (Figure 10C). In addition, I found that low platelet and elevated hematocrit markers of DHF in the DV2-αDV3 group confirmed the tendency to recover when treated with recombinant IL-12 (Figures 11A and B). There has been reported that massively enhanced infection of liver sinusoidal endothelial cells (LSECs) occurred in mice infected with ADE of DV2 (87). Therefore, I examined that the tight junction (ZO-1) and adherent junctions of vessel (E-cadherin and N-cadherin) proteins from

lungs lysates of mice were decreased in the DV2-αDV3 group and were recovered in DV2-αDV3 group treated with recombinant IL-12 (Figure 11C). Because mice infected with 10^5 FFU of DV2 did not die, I confirmed the survival rate and body weight change of lethal dose of DV2 by infection with 10^7 FFU of DV2. All mice infected with 10^7 FFU of DV2 died at day 6 post-infection. However, mice treated with recombinant IL-12 showed survival of 100% and did not reduce the body weight compared with 10^7 DV2 group (Figure 11D). Finally, I confirmed the gastrointestinal bleeding in the severe DV-infected group, and recombinant IL-12 treatment alleviated the gastrointestinal bleeding (Figure 11E). Taken together, recombinant IL-12 treatment effectively alleviated DHF in mice model of severe DV infection.

Severe DV infection selectively represses IL-12p35 production in inflammatory macrophages.

In my study, I established severe DV infection conditions according to several conditions in inflammatory macrophages. Severe DV conditions include: 1) high dose of DV infection (30 MOI of DV2), 2) ADE of DV infection (DV2-αDV3, DV2-E60). In addition, an E60-N297Q antibody that cannot bind to FcγR was used as a negative control of FcγR signaling (description of the antibodies is described in the Method and Material section). To find out why IL-12 was decreased in *in vitro* model of severe DV2, I measured the various cytokines of inflammatory macrophages infected with DV2 by ELISA. I thought severe DV2-mediated receptors

(CLEC5A and FcγR) suppressed the mRNA level of IL-12p35. I confirmed that severe DV infection increased the production of TNF-α, IL-6, and IL-12p40 but not IL-12p70 (Figure 12A). Next, I examined the lack of IL-12p70 expression. IL-12p70 comprises of IL-12p35 and IL-12p40 subunits. Severe DV-infected THP-1 produced IL-12p40 (Figure 12A), indicating that IL-12p70 expression is restricted at the level of IL-12p35. After 12 hours after severe infection in THP-1, I confirmed the mRNA levels of IL-12p35 and IL-12p40. In the 1 MOI of DV infection, the mRNA levels of IL-12p35 and IL-12p40 were increased, but only the mRNA levels of IL-12p35 was decreased in the 30 MOI of DV infection and the ADE of DV infection (DV2-αDV3, DV2-E60). Interestingly, IL-12p35 was increased in the E60-N297Q infection that cannot bind to FcγR than in the DV2-E60 (Figure 12B). These data strongly suggest that severe DV infection actively suppresses IL-12p35 production through FcγR signaling.

Severe dengue virus infection suppresses nuclear IRF-1 activity to block IL-12p35 nucleosome remodeling.

IL12A transcription is rigidly controlled in resting cells, and the *IL12A* promoter is assembled into stable nucleosomes, whereas upon stimulation, repositioning of nucleosome 2 (nuc-2) allows binding of, among others, NF-κB and subsequent transcriptional initiation by RNA polymerase II (RNAPII) (88). To confirm whether NF-κB p65, RNAPII, and IRF1 recruit into the nucleus upon severe DV2 infection, it was determined by

ChiP assay. I observed that, although severe DV2 infection interfered with NF-κB p65 recruitment to the *IL12A* promoter (Figure 13A), severe DV2 infection stimulation did not abrogate nuclear translocation of p65 (Figure 13B). Indeed, severe DV infection induced nuclear translocation of p65, p52, p50, RelB, and c-Rel (Figure 13B), a hallmark of NF-κB signaling (89). Moreover, RNAPII and IRF1 recruitment to the *IL12A* promoter was almost completely abolished but not DV2-N297Q infection (Figure 13A). Since these data suggest that FcγR signaling interferes with *IL12A* transcription prior to RNAPII and NF-κB binding, I next examined whether severe DV infection interfered with *IL12A* nucleosome remodeling. Severe DV infection did not induce *IL12A* nucleosome remodeling, whereas 1 MOI of DV infection and DV2-N297Q infection evoked complete remodeling (Figure 13C). These results strongly suggest that ADE of DV infection-induced FcγR signaling inhibits IL-12p35 expression by interfering with nucleosome remodeling events indispensable for transcriptional activation at the *IL12A* promoter. The nuc-2 promoter region of *IL12A* contains an IFN-stimulated response element (ISRE) that can be bound by IRF1 (90). To determine whether IRF1 interacted with the *IL12A* in the nucleus, I made IRF1 silencing macrophages. Macrophages were transfected with siRNA using transfection reagent as described in Materials and Methods. Next, I found that IRF1 silencing abrogated IL-12p35 expression in response to all of ADE of DV2 infection (Figure 13D).

CLEC5A and FcγR signaling suppress IL-12p35 expression via PI3K and AKT.

I established severe DV infection conditions (high dose of DV2 infection and ADE of DV infection) in this study and confirmed the regulation of IL-12p35 by the downstream signaling pathways of CLEC5A and FcγR, respectively. The previous study demonstrated that the interaction between DV and CLEC5A was relatively weak because CLEC5A had a low binding affinity to DV (91). I thought a high dose of DV infection could trigger activation of the CLEC5A signaling pathway, so I confirmed that phosphorylation of DAP12 was increased in 30 MOI of DV2 infection (Figure 14A). In addition, the expression level of IL-12p35 was also decreased in 30 MOI of DV2 infection. However, it was confirmed that the expression level of IL-12p35 increased in the CLEC5A silencing group by siRNA transfection (Figure 14B). These results showed that CLEC5A regulated IL-12p35 transcription at a high dose of DV2 infection. Later, I checked that BCL10, MALT1, and CARD9 were commonly involved in the CLEC5A and FcγR signaling pathways (92, 93). Then, these genes were silenced, IL-12p35 was increased in the 30 MOI of DV2 infection and the ADE of DV2 infection (Figures 14C and 14D). Finally, I examined that the phosphorylation of PI3K, AKT, and MDM2 was increased in severe DV2 infection (Figure 14E). These results indicated that CLEC5A and FcγR suppressed severe DV infection-induced IL-12p35 expression in inflammatory macrophages by activation of PI3K-AKT signaling through a CARD9-BCL10-MALT1 dependent pathway.

Severe dengue virus infection induces proteasomal degradation of nuclear IRF1 via MDM2.

I next investigated whether FcγR signaling triggering affected *IL12A* nucleosome remodeling by interfering with IRF1 activation. I found that both 1 MOI of DV2 and DV2-N297Q infection induced nuclear translocation of IRF1 (Figure 15A). Remarkably, infection with ADE of DV completely abrogated nuclear IRF1 accumulation (Figure 15A). IRF1 steady-state levels are tightly controlled by a balance between synthesis and ubiquitin-mediated proteolysis (94). Then, I prepared nuclear extracts in the presence of MG-132 to block degradation to determine whether MDM2 interacts with IRF1 within the nucleus. Treatment with proteasome inhibitor MG-132 reversed the block in nuclear IRF1 of high dose (30 MOI) and ADE infection of DV2 (Figure 15B). Also, I found that nuclear IRF1 immunoprecipitated together with MDM2 in both high dose of infection (DV2 30 MOI) and ADE of DV2 infection (DV2-αDV3), but not 1 MOI of DV2 infection in inflammatory macrophages (Figure 15B). It indicated that IRF1 was indeed targeted for proteasomal degradation by CLEC5A and FcγR. Also, I explored a possible MDM2 contribution. Remarkably, MDM2 silencing completely abrogated CLEC5A and FcγR-mediated IL-12p35 suppression (Figure 15C).

Administration of MDM2 inhibitor did not protect dengue hemorrhagic fever in IFNAR KO mice

Previously, I confirmed that the translocation of IRF1 was inhibited by MDM2-mediated. Therefore, I expected that hemorrhagic fever would be reduced when the MDM2 inhibitor (Nutlin-3A) was treated in IFNAR KO-infected mice, similar to the therapeutic effect of recombinant IL-12. In my animal infection model, the inoculation of DV was a sub-lethal dose (10^5 FFU per mouse), and after 6 days of infection, the body weight was restored, and the survival rate was 100%. However, the ADE of DV infection (DV2-αDV3) group showed a 75% survival rate, and the weight recovery was not as good as the DV infection group (Figures 16A and B). Unexpected, MDM2 inhibitor treatment showed a worse 60% survival rate and did not regain body weight (Figures 16A and B). These results were consistent with the increase in MMP-9 in the MDM2 inhibitor-treated group (Figure 16C). Because MDM2 inhibitor plays a role in preventing the binding of MDM2 to p53, this might increase more MDM2, which appears to have unknown side effects. Therefore, I think that it is necessary to develop molecules that can regulate MDM2 at the transcriptional level (microRNA, other binding inhibitors, etc.). I expect that transcriptional repression of MDM2 or protein-binding inhibitors can increase the production of IL-12 by increasing the translocation of IRF1. These innovative therapeutic approaches have the therapeutic effect of DHF as well as the anti-viral effect.

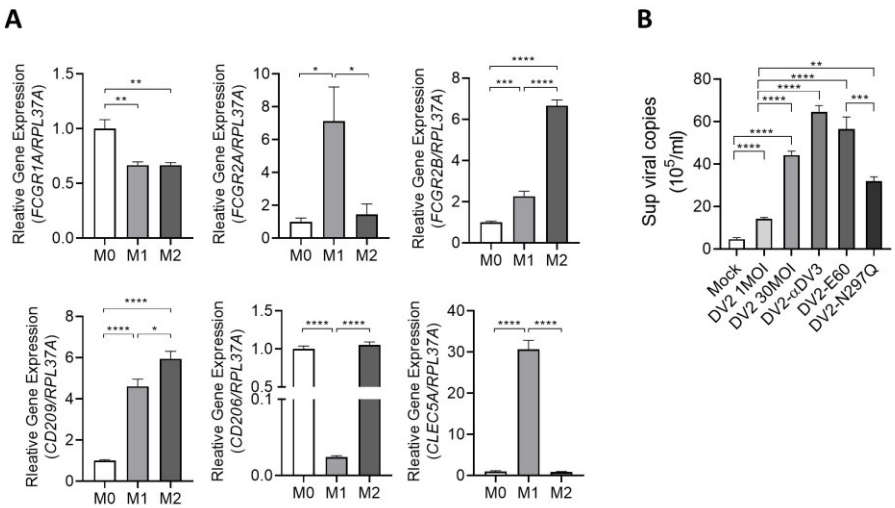

Figure 7. mRNA gene expression of receptors in different types of THP-1 cells and viral RNA in inflammatory macrophages. (A) THP-1 cells were differentiated by various types of macrophages (M0, M1, and M2) as described by Materials and Method. The mRNA level of *FCGR1*, *FCGR2A*, *FCGR2B*, *CD209*, *CD206*, and *CLEC5A* of THP-1 was determined by RT-qPCR, normalized to *RPL37A*. Data are presented as the mean ± SEM. $*P < 0.05$, $**P < 0.01$, $***P < 0.001$, $****P < 0.0001$ by the one-way ANOVA with multiple comparisons test. **(B)** THP-1 cells were infected with DV2 at various MOIs (1 or 30) or infected with DV2/antibody complex (anti-DV3, hE60, or hE60-N297Q). The culture supernatant was harvested at 48 post-infection time. The total RNA extracted from DV genome copy number was determined by RT-qPCR. Data are presented as the means ± SEM and are representative of two independent experiments. $**P < 0.01$, $***P < 0.001$, $****P < 0.0001$ by the one-way ANOVA with multiple comparisons test.

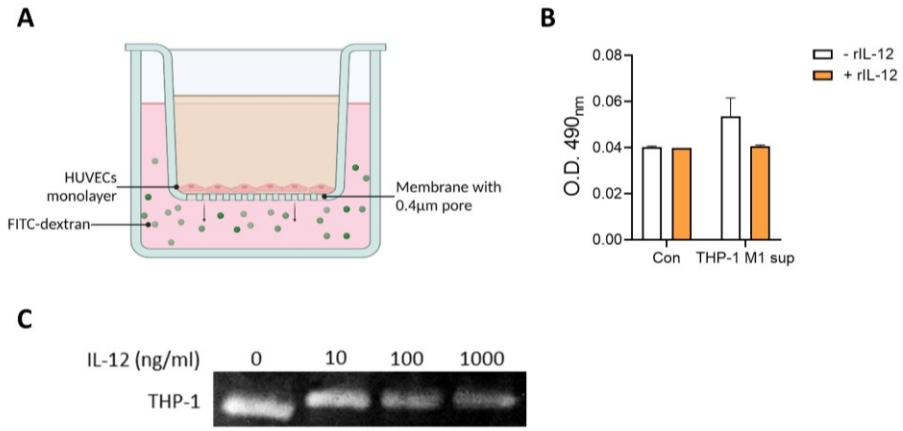

Figure 8. Treatment of recombinant IL-12 inhibits vessel permeability and MMP-9 activity. **(A)** Schematic representation of the transwell assay system. To mimic the endothelium *in vivo*, HUVECs were seeded on matrigel-coated 0.4 μm pore size filters in the upper well, as described in the Material and Methods section. As a permeability indicator, 70 kDa FITC-dextran (1 mg/mL) was used and introduced into the lower chamber along with the permeability-inducing agent. The permeability was quantified as fluorescence units of the FITC that passed from the lower chamber into the upper chamber and was plotted over time after the addition of the reagents. **(B)** FITC-dextran transwell assay of HUVEC monolayers treated with culture medium (Con), cell supernatant of M1 type THP-1 (THP-1 M1 sup) treated with 10 ng/mL of recombinant IL-12 or not. 10 minutes after adding FITC-dextran, the fluorescence intensity of the medium in the lower compartments was measured by the fluorescent microplate reader at 490 nm. **(C)** Gelatin zymography of MMP-9 activity in the culture medium accumulated for 72 hours of M1

type THP-1 treated with 0, 10, 100, and 1,000 ng/mL of recombinant IL-12.

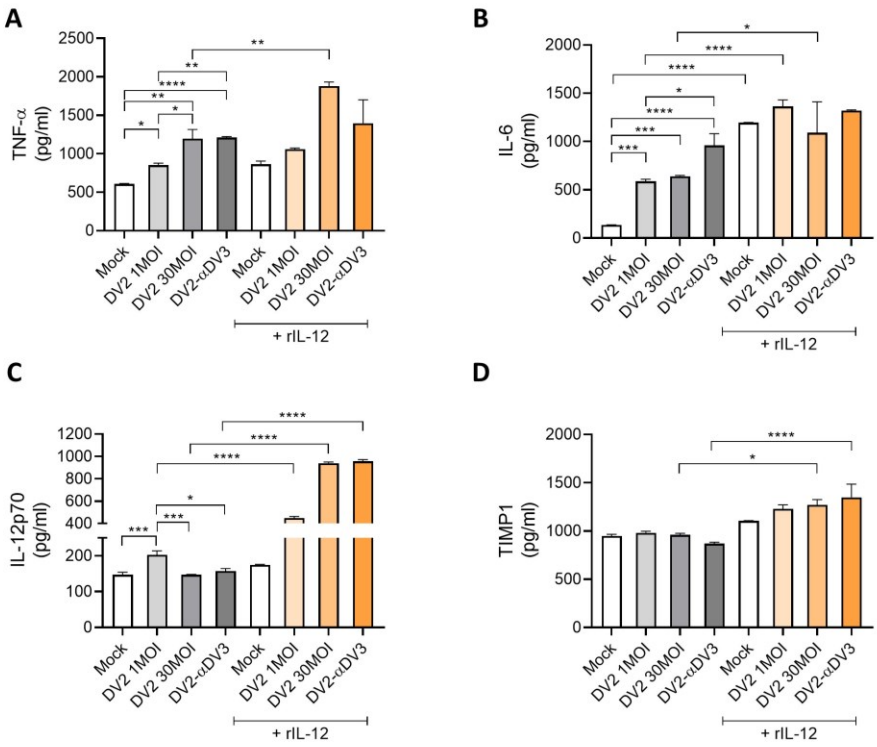

Figure 9. Treatment of recombinant IL-12 increases the pro-inflammatory cytokines and TIMP-1 in THP-1 infected with severe DV2. (A-D) Cytokine secretion in supernatants of THP-1 72 hours after infection with severe DV2 treated with recombinant IL-12 or not. TNF-α **(A)**, IL-6 **(B)**, IL-12p70 **(C)**, and TIMP-1 (**D**) were measured by ELISA. Data are presented as the means ± SEM and are representative of two independent experiments. $*P < 0.05$, $**P < 0.01$, $***P < 0.001$, $****P < 0.0001$ by the one-way ANOVA with multiple comparisons test.

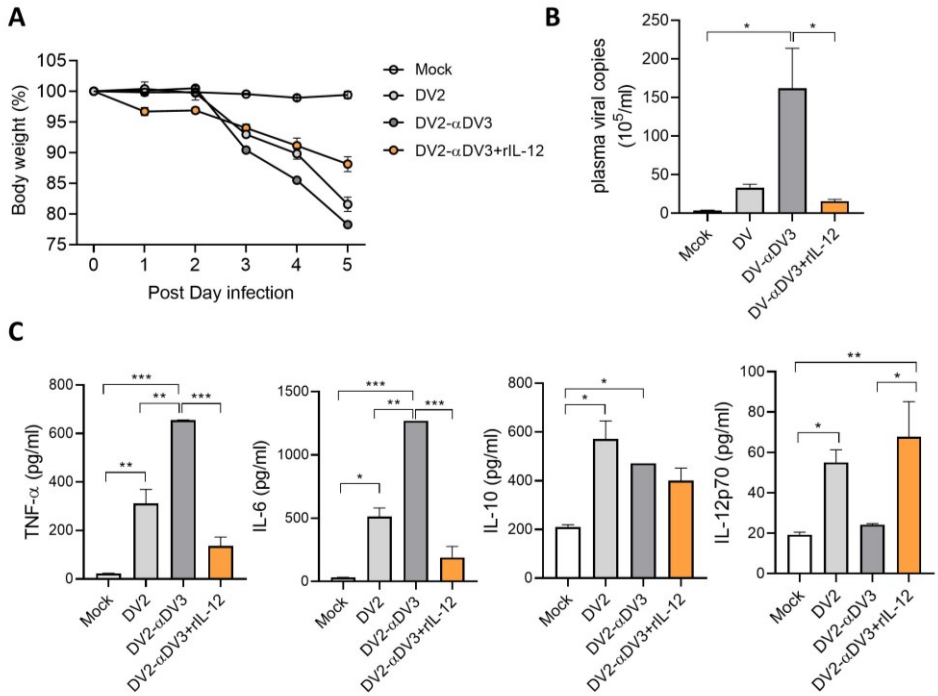

Figure 10. Treatment of recombinant IL-12 significantly reduces the pro-inflammatory cytokines and viral RNA in mice with a severe infection of DV2. Mice were injected intraperitoneally with PBS, or anti-DV3, in a total volume of 200 μL, then infected 24 hours later with 10^5 FFU of DV2 by iv injection into the tail vein in a total volume of 100 μL. Mice were treated with 50 μg/kg of recombinant IL-12 twice. On day 5 post-infection, mice were fully anesthetized with ketamine/xylazine. **(A)** Mouse body weight change of infected mice (n = 5 per group) after recombinant IL-12 treatment. **(B)** Viral RNA from the plasma of mice was quantified using RT-qPCR in mice infected with severe DV2 in the presence or absence of recombinant IL-12 treatment (n = 5 per group). $*P < 0.05$ by the one-way ANOVA with multiple comparisons test. **(C)** Cytokines (TNF-α, IL-6, IL-10, and IL-12p70) from the plasma of mice were measured by

ELISA (n = 5 per group). Data are presented as the means ± SEM. $*P < 0.05$, $**P < 0.01$, $***P < 0.001$ by the one-way ANOVA with multiple comparisons test.

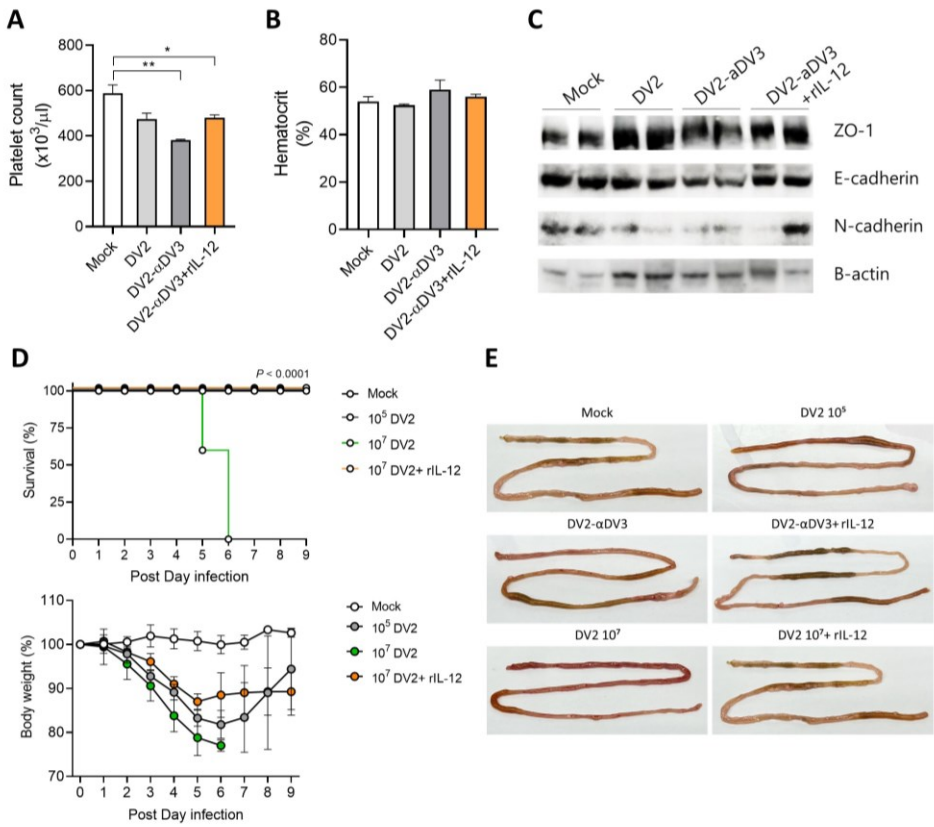

Figure 11. Treatment of recombinant IL-12 significantly inhibits dengue hemorrhagic fever in mice with a severe infection of DV2. Mice were injected intraperitoneally with PBS, or anti-DV3 antibody, in a total volume of 200 μL, then infected 24 hours later with 10^5 or 10^7 FFU of DV2 by iv injection into the tail vein in a total volume of 100 μL. Mice were treated with 50 μg/kg of recombinant IL-12 twice. On day 5 post-infection, mice were fully anesthetized with ketamine/xylazine. **(A, B)** Platelet counts and hematocrit from plasma of mice infected with severe DV2 on day 5 post-infection (n = 5 per group). Data are presented as the means ± SEM. $*P < 0.05$ and $**P < 0.01$ by the one-way ANOVA with multiple comparisons test. **(C)** The tight junction (ZO-1) and adherent

junctions of vessel (E-cadherin and N-cadherin) proteins from the lung lysates of mice were measured by Western blot (n = 2 per group). **(D)** Survival rate and body weight change of DV2 infected mice (n = 5 per group) after recombinant IL-12 treatment. $P < 0.001$ by the log-rank test with multiple comparisons test. **(E)** On day 5 post-infection, gastrointestinal bleeding in the small intestine in the presence or absence of recombinant IL-12 treatment. Tissues from one representative animal per group are shown.

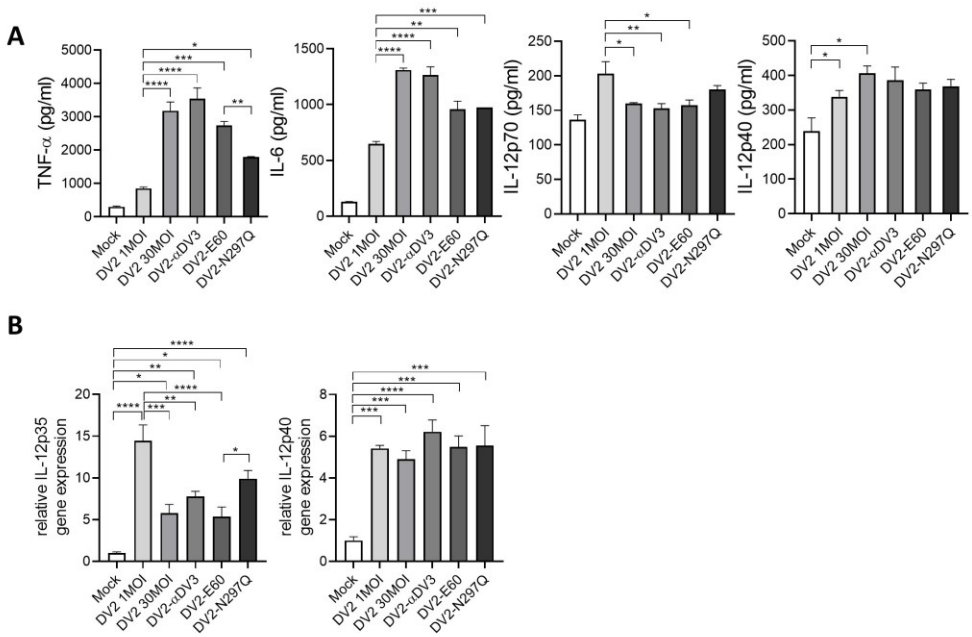

Figure 12. Severe infection of DV2 increases pro-inflammatory cytokines but not IL-12p70. (A) Cytokine secretion (TNF-α, IL-6, IL-12p70, and IL-12p40) in supernatants of THP-1 24 hours after infection with severe DV2 was measured by ELISA. *$P < 0.05$, **$P < 0.01$, ***$P < 0.001$, ****$P < 0.0001$ by the one-way ANOVA with multiple comparisons test. **(B)** mRNA expression of IL-12p35 and IL-12p40 of THP-1 12 hours after infection with severe DV2 was measured by RT-qPCR, normalized to *RPL37A*. Data are presented as the means ± SEM and are representative of two independent experiments. *$P < 0.05$, **$P < 0.01$, ***$P < 0.001$, ****$P < 0.0001$ by the one-way ANOVA with multiple comparisons test.

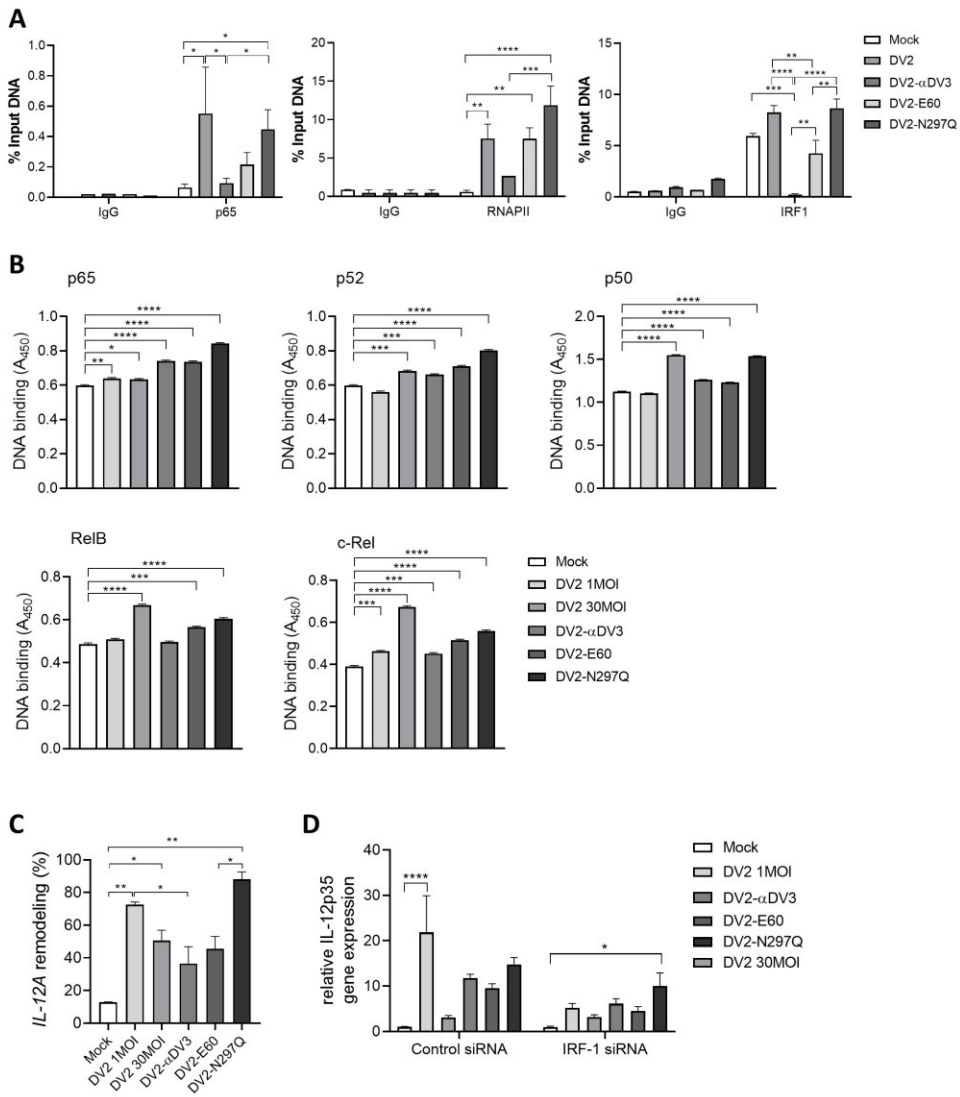

Figure 13. IRF1 blocks *IL12A* transcription by inhibition of nucleosome remodeling. **(A)** p65, and RNA polymerase II (RNAPII), and IRF1 recruitment to NF-κB, TATA box, and interferon-sensitive response element (ISRE) binding motifs of the *IL12A* promoter in THP-1 24 hours after infection with severe DV2 were determined by ChIP assay. IgG indicates negative control. $*P < 0.05$, $**P < 0.01$, $***P < 0.001$, $****P < 0.0001$ by the two-way ANOVA with multiple comparisons test. **(B)** NF-

κB subunit activation in nuclear extracts of THP−1 24 hours after infection with severe DV2 measured by DNA binding ELISA. $*P < 0.05$, $**P < 0.01$, $***P < 0.001$, $****P < 0.0001$ by the one−way ANOVA with multiple comparisons test. **(C)** *IL12A* nucleosome remodeling in THP−1 24 hours after infection with severe DV2 was determined by ChART assay and normalized to *RPL37A*. $*P < 0.05$, $**P < 0.01$, $***P < 0.001$, $****P < 0.0001$ by the one−way ANOVA with multiple comparisons test. **(D)** IL−12p35 mRNA expression of THP−1 12 hours after infection with severe DV2, after IRF1 silencing, was measured by RT−qPCR and normalized to *RPL37A*. Data are presented as the means ± SEM and are representative of two independent experiments. $*P < 0.05$, $**P < 0.01$, $***P < 0.001$, $****P < 0.0001$ by the two−way ANOVA with multiple comparisons test.

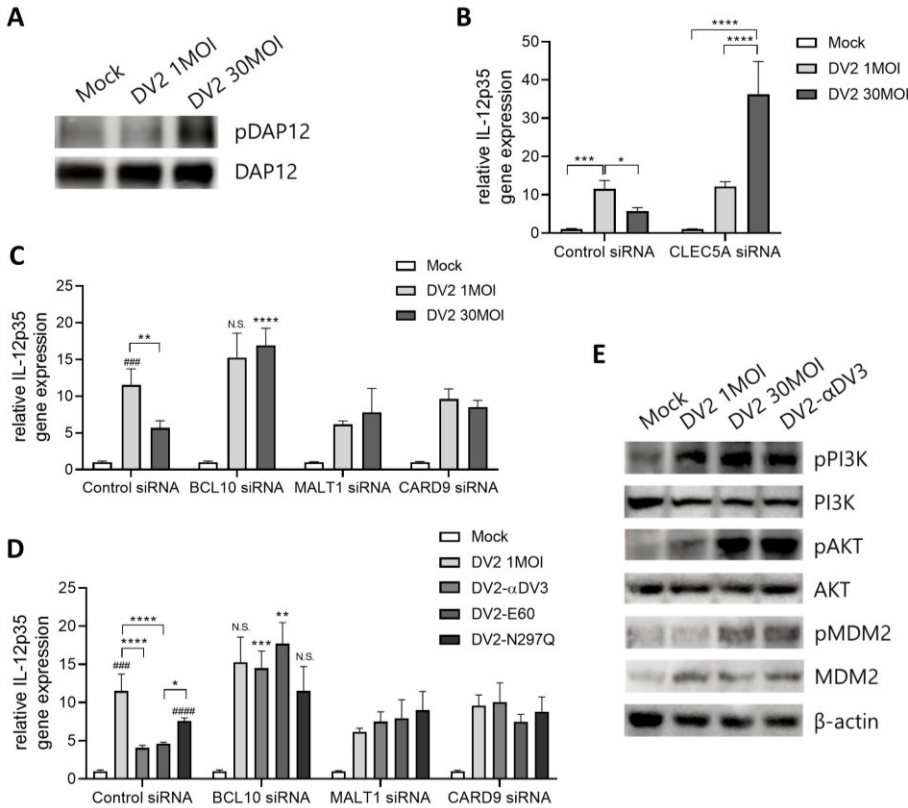

Figure 14 CLEC5A and FcγR signaling suppress IL-12p35 expression via PI3K and PKB. (A) DAP12 phosphorylation in the total lysates of THP-1 2 hours after infection with severe DV2 was measured by Western blot. **(B)** IL-12p35 mRNA expression of THP-1 12 hours after infection with severe DV2, after CLEC5A silencing, was measured by RT-qPCR and normalized to *RPL37A*. Data are presented as the means ± SEM and are representative of two independent experiments. $*P < 0.05$, $***P < 0.001$, $****P < 0.0001$ by the two-way ANOVA with multiple comparisons test. **(C-D)** IL-12p35 mRNA expression of THP-1 12 hours after infection with severe DV2, after BCL10, MALT1, and CARD9 silencing, were measured by RT-qPCR and normalized to *RPL37A*. Data are presented as

the means ± SEM and are representative of two independent experiments. $*P < 0.05$, $***P < 0.001$, $****P < 0.0001$, $\#\#\#P < 0.001$, $\#\#\#\#P < 0.0001$ compared with Mock by the two-way ANOVA by the two-way with multiple comparisons test. N.S.: not significant. **(E)** Phosphorylation of PI3K, AKT, and MDM2 in the total lysates of THP-1 24 hours after infection with severe DV2 was measured by Western blot.

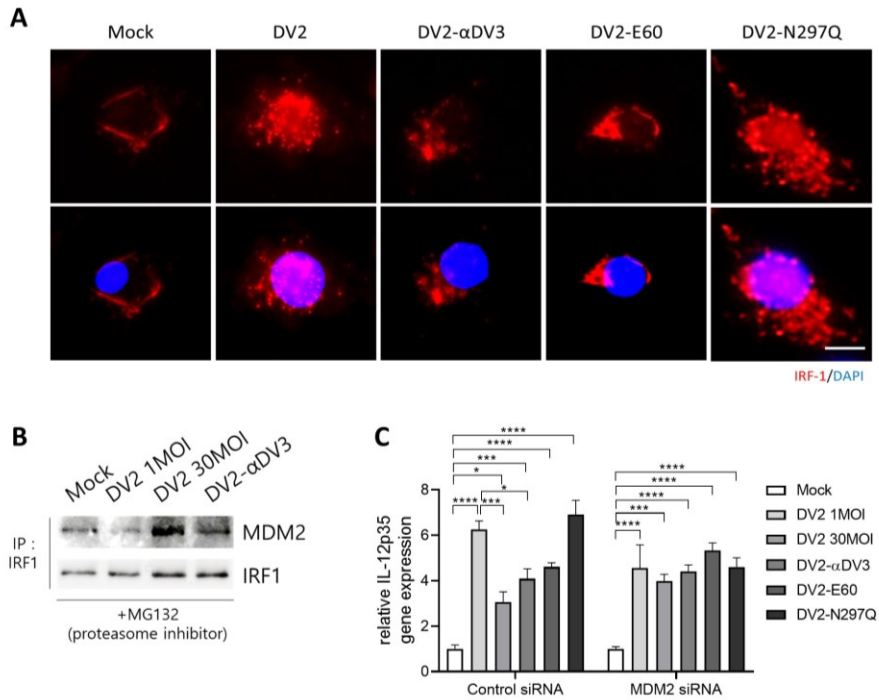

Figure 15. CLEC5A and FcγR signaling induce proteasomal degradation of nuclear IRF1 via Mdm2. **(A)** IRF1 nuclear translocation THP−1 24 hours after infection with severe DV2 immunofluorescence microscopy (IRF1, red; DAPI, blue) Scale bar; 20 μm. **(B)** MDM2 immunoprecipitated together with IRF1 (IP) from nuclear extracts of THP−1 24 hours after infection with severe DV2 was determined by immunoblotting. NE was prepared in the presence of proteasome inhibitor MG−132 to block protein degradation. **(C)** IL−12p35 mRNA expression by THP−1 24 hours after infection with severe DV2, after MDM2 silencing, was measured by RT−qPCR and normalized to *RPL37A*. Data are presented as the means ± SEM and are representative of two independent experiments. $*P < 0.05$, $***P < 0.001$, $****P < 0.0001$ by the two−way ANOVA with multiple comparisons test.

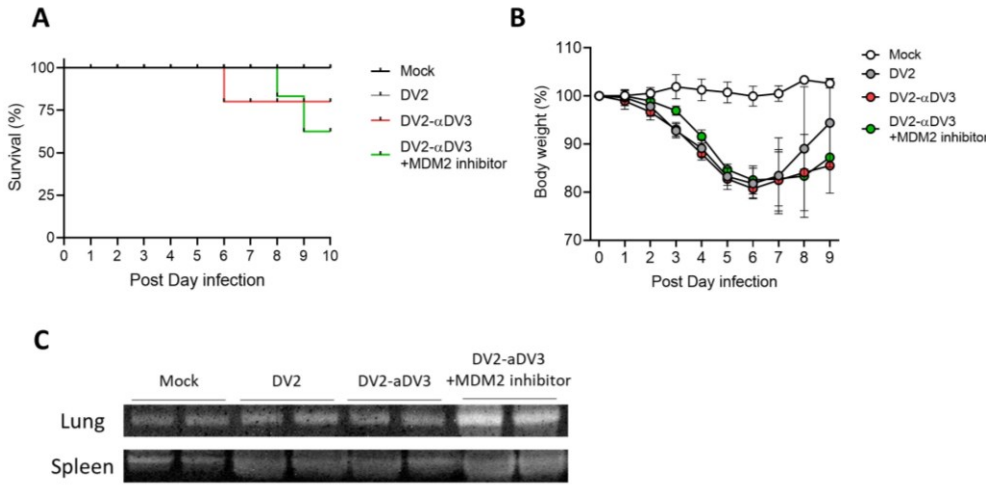

Figure 16. Treatment of MDM2 inhibitor does not alleviate dengue hemorrhagic fever in mice with a severe infection of DV2. Mice were injected intraperitoneally with PBS, or anti-DV3, in a total volume of 200 μL, then infected 24 hours later with 10^5 FFU of DV2 by iv injection into the tail vein in a total volume of 100 μL. Mice were treated with 1 mg/kg of MDM2 inhibitor (Nutlin-3A) twice. On day 5 post-infection, mice were fully anesthetized with ketamine/xylazine. Survival **(A)** and body weight change **(B)** of infected mice (n = 5 per group) after MDM2 inhibitor treatment. **(C)** Gelatin zymography of MMP-9 activity proteins from lungs and spleen lysates of mice (n = 2 per group) in the presence or absence of MDM2 inhibitor treatment.

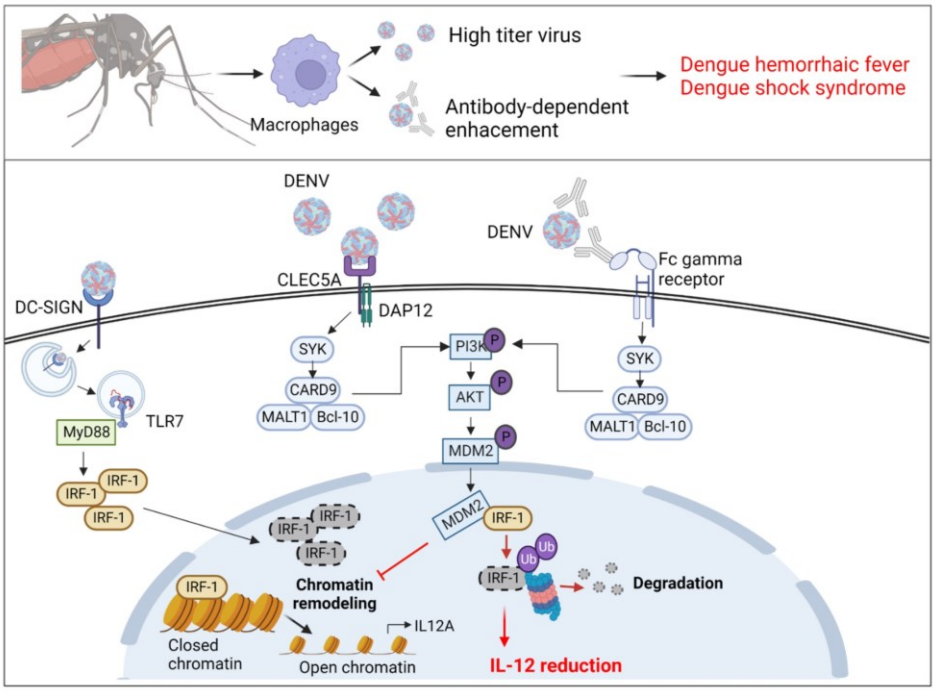

Figure 17. Schematic figure of the mechanism of macrophage signaling events involved in producing IL-12 in the dengue virus infection. The mechanism of human macrophage signaling events involves the production of IL-12. The CLEC5A and FcγR signaling interfere with nuclear IRF1 activity and abrogated IRF1-mediated *IL12A* remodeling. This study demonstrates that severe DV infection (e.g., high dose of DV infection or ADE of DV infection) triggers CLEC5A or FcγR, which leads to specific degradation of IRF1, thereby suppressing *IL12A* transcription in macrophages. CLEC5A and FcγR signaling lead to E3 ubiquitin ligase MDM2-dependent proteasomal degradation of IRF1 in the nucleus. Furthermore, a high dose of DV infection and ADE of DV infection induces vascular permeability *in vitro* and *in vivo* by down-regulating IL-12 production to induce MMP-9.

DISCUSSIONS

For the first time, this study showed that severe DV infection down-regulated IL-12 production in inflammatory macrophages via activation of CLEC5A or FcγR. To the best of our knowledge, this is the first report to show the role of IL-12 in severe DV infection, which will be important for vascular permeability in dengue victims. In addition, it has been shown that IL-12 is associated with anti-angiogenesis, but little is known about vascular permeability.

Dendritic cells and macrophages are the primary targets of DV infections (25). Whereas infected dendritic cells undergo apoptosis, infected macrophages survive for at least 45 days and secrete multiple cytokines and chemokines from infection in target organs (26). So I thought macrophages were the major source of IL-12 and other pro-inflammatory cytokines and chemokines, although my study did not show that IL-12 was specifically regulated in macrophages using macrophage-specific IL-12 knock-out mice.

The characteristic symptoms of DHF/DSS patients are characterized by increased capillary permeability, severe plasma leakage, respiratory distress, and extensive pleural effusion (95). However, the underlying molecular mechanism has not been elucidated. Recently, preexisting antibodies and increased cytokine levels in patients have played an important role in the pathogenesis of DHF/DSS (25, 96). Also, non-structural protein 1 (NS1) of DV was increased in the plasma of DHF/DSS

patients (97). Based on previous clinical results, I established severe DV infection causing DHF/DSS model by infecting with high dose (30 MOI) of DV2 or ADE infection of DV2 in THP-1 derived macrophages and IFNAR KO mice.

Macrophages use the virus pattern recognition receptor CLEC5A instead of MR and DC-SIGN to secrete pro-inflammatory cytokines (91). Furthermore, a high dose of DV infection induces DAP12 phosphorylation to the secretion of pro-inflammatory cytokines (80, 86, 91). On the other hand, many studies demonstrated the critical role of Fc-gamma receptor 2A (FcγR2A). Activation of FcγR2A induces phosphorylation of spleen tyrosine kinase (Syk), inducing cellular activation through phospholipase c gamma (PLCγ) and phosphoinositide 3-kinase (PI3K) signaling pathways, resulting in the production of pro-inflammatory signaling (98). Interestingly, the production of inflammatory cytokines by pathogens was exaggerated through the molecular mechanisms of Toll-like receptors (TLRs) and ITAM-containing proteins such as DAP12 or the FcγR-chain crosstalk and synergy (99, 100). However, unlike other inflammatory cytokines, IL-12 was down-regulated in severe DV infection, suggesting the possibility that IL-12 was regulated by receptor-mediated ITAM signaling independent of TLR signaling.

Until recently, little attention has been paid to how IRF1 maintains a basal level of protection against viruses. Daisuke Yamane *et al.* showed that IRF1 acted independently of mitochondrial antiviral signaling (MAVS)

protein, IRF3, and signal transducer and activator of transcription 1 (STAT1)-dependent signaling to provide intrinsic antiviral protection. Based on the previous studies, the important findings of my study are the crucial role of IRF1 in *IL12A* nucleosome remodeling and IL-12p35 synthesis by different receptor CLEC5A and FcγR sensing DV. Also, I found that IRF1-mediated *IL12A* nucleosome remodeling of the proximal *IL12A* promoter in response to CLEC5A and FcγR activation allowed NF-κB subunit p65 and RNAPII recruitment, resulting in productive *IL12A* transcription (Figure 13).

My findings revealed that CLEC5A and FcγR activation exerted their suppressive effect by directing proteolytic breakdown of nuclear-localized IRF1 via CARD9-BCL10-MALT1-dependent activation of a PI3K-AKT cascade. I also identified E3 ubiquitin ligase MDM2 as the downstream effector: CLEC5A and FcγR-induced AKT activation led directly to MMD2 phosphorylation and nuclear translocation (Figures 14 and 15). MDM2 is a major negative regulator of numerous proteins involved in transcriptional regulation, most notably p53 and FOXO tumor suppressors, under conditions of physiological stress (101, 102).

Another important finding of my study is the crucial and non-redundant role of IL-12 in severe DV infection models *in vitro* and *in vivo*. I found that IL-12 was crucial for not only inducing IFN-γ production and triggering $CD4^+$ T cells to differentiate into type 1 T helper (Th1)

cells but also attenuating vascular permeability through down-regulating of MMP-9.

My research showed that although the amount of IL-12 produced by macrophages after viral infection was lower than that of other pro-inflammatory cytokines (e.g., TNF-α and IL-6), MMP-9 regulation and viral clearance were remarkable. While p35 is unique to IL-12, p40 is shared with IL-23 (consisting of p40 and p19 subunits), another inflammatory cytokine required for the development of Th17 T cell immunity (103). In addition, p40 is normally secreted in macrophages or other cells, whereas p35 is precisely regulated, and transcription is initiated only by stimuli such as LPS and IFN-γ. It was reported that IRF1-deficient macrophages had a selective impairment in mRNA synthesis of IL-12 p35 but not the p40 gene and a strong deficiency in the production of IL-12 p70 but not the p40 (90). These results were consistent with my findings that severe DV infection precisely regulated IRF1-mediated IL-12p35 transcription by receptor signaling in macrophages.

Also, I determined that recombinant IL-12 had a therapeutic effect on mice models infected with severe DV (high dose infection or ADE infection). Mice treated with recombinant IL-12 showed rapidly regained body weight and low levels of viral RNA compared to mice infected with severe DV. Also, treatment of recombinant IL-12 reduced the vascular permeability in the lungs of mice infected with severe DV. Because of this

remarkable antiviral effect in preclinical animal models, I considered the application of recombinant IL-12 treatment as an immunotherapy for viral diseases. Unfortunately, IL-12's antitumor efficacy in preclinical models has yet to be replicated in humans. Early clinical trials in the mid-1990s showed that systemic delivery of IL-12 incurred dose-limiting toxicities (104). IL-12, like most cytokines, functions locally through paracrine and autocrine mechanisms. Therefore, the ideal targets of IL-12 immunotherapy are not leukocytes in circulation but immune cells within the viral target organ, including activated but exhausted T cells and macrophages. I thought the side effects would be reduced if the drug was delivered to target macrophages, the target cells of the DV, in target organs. In addition, unlike cancer treatment regimens that require continuous treatment, it is expected that DHF treatment would not be. This is because DHF occurs rapidly within 7 days of DF symptoms, and death or recovery from DHF is determined within 2 weeks. Thus to achieve the regular role of IL-12, IL-12 immunotherapy is considered within the first 7 days of the onset of symptoms of DHF.

My study showed that the MDM2 inhibitor did not protect against hemorrhage of mice infected with severe DV (Figure 16). Contrary to my expectation, Nutlin-3A, an MDM2 inhibitor, did not reduce MMP-9 activity in the animal model. Blocking of binding sites by Nutlin-3A led to an accumulation of MDM2 that occurred due to a feedback loop triggered by the transcriptional activation of p53 (105). Other studies have reported that TNF-α levels were increased following MDM2 inhibitor treatment

(106). I thought these uncontrolled events occurred after MDM2 inhibitor treatment. Therefore, I thought recombinant IL-12 might be used as a promising therapeutic approach for treating DHF/DSS patients, but new molecules regulating the transcriptional level of MDM2 should be developed for controlling IRF1.

Overall, my study has identified an essential role for IRF1 in regulating the transcription of IL-12 to virulent severe DV associated with pathological vascular permeability (Figure 17). Therapeutic targeting of IRF1 may therefore prove beneficial not only in the treatment of hemorrhagic fever but also in diseases marked by uncontrolled IL-12-driven inflammation.

Reference

1. J. M. Zhang, J. An, Cytokines, inflammation, and pain. *Int Anesthesiol Clin* **45**, 27-37 (2007).
2. C. Gao *et al.*, Proinflammatory cytokines are associated with prolonged viral RNA shedding in COVID-19 patients. *Clin Immunol* **221**, 108611 (2020).
3. T. H. Mogensen, S. R. Paludan, Molecular pathways in virus-induced cytokine production. *Microbiol Mol Biol Rev* **65**, 131-150 (2001).
4. C. Centers for Disease, Prevention, Estimates of deaths associated with seasonal influenza --- United States, 1976-2007. *MMWR Morb Mortal Wkly Rep* **59**, 1057-1062 (2010).
5. S. S. Shrestha *et al.*, Estimating the burden of 2009 pandemic influenza A (H1N1) in the United States (April 2009-April 2010). *Clin Infect Dis* **52 Suppl 1**, S75-82 (2011).
6. S. Gordon, P. R. Taylor, Monocyte and macrophage heterogeneity. *Nat Rev Immunol* **5**, 953-964 (2005).
7. A. Sica, A. Mantovani, Macrophage plasticity and polarization: in vivo veritas. *J Clin Invest* **122**, 787-795 (2012).
8. F. O. Martinez, S. Gordon, The M1 and M2 paradigm of macrophage activation: time for reassessment. *F1000Prime Rep* **6**, 13 (2014).
9. L. A. Perrone, J. K. Plowden, A. Garcia-Sastre, J. M. Katz, T. M. Tumpey, H5N1 and 1918 pandemic influenza virus infection results in early and excessive infiltration of macrophages and neutrophils in the lungs of mice. *PLoS Pathog* **4**, e1000115 (2008).
10. J. Wilkinson, M. Radkowski, J. M. Eschbacher, T. Laskus, Activation of brain macrophages/microglia cells in hepatitis C infection. *Gut* **59**, 1394-1400 (2010).
11. H. A. Imad *et al.*, Cytokine Expression in Dengue Fever and Dengue Hemorrhagic Fever Patients with Bleeding and Severe Hepatitis. *Am J Trop Med Hyg* **102**, 943-950 (2020).
12. B. S. Bender, P. A. Small, Jr., Influenza: pathogenesis and host defense. *Semin Respir Infect* **7**, 38-45 (1992).
13. N. L. La Gruta, K. Kedzierska, J. Stambas, P. C. Doherty, A question of self-preservation: immunopathology in influenza virus infection. *Immunol Cell Biol* **85**, 85-92 (2007).
14. Q. Liu, Y. H. Zhou, Z. Q. Yang, The cytokine storm of severe influenza and development of immunomodulatory therapy. *Cell Mol Immunol* **13**, 3-10 (2016).
15. D. J. Arora, M. Houde, Modulation of murine macrophage responses stimulated with influenza glycoproteins. *Can J Microbiol* **38**, 188-192 (1992).
16. M. Chomik, Interferon induction by influenza virus: significance of neuraminidase. *Arch Immunol Ther Exp (Warsz)* **29**, 109-104 (1981).
17. I. Puc *et al.*, Cytokine Signature of Dengue Patients at Different Severity of the Disease. *Int J Mol Sci* **22** (2021).

18. Y. H. Huang *et al.*, Dengue virus infects human endothelial cells and induces IL-6 and IL-8 production. *Am J Trop Med Hyg* **63**, 71-75 (2000).
19. O. Tatar *et al.*, Effect of bevacizumab on inflammation and proliferation in human choroidal neovascularization. *Arch Ophthalmol* **126**, 782-790 (2008).
20. M. Norelli *et al.*, Monocyte-derived IL-1 and IL-6 are differentially required for cytokine-release syndrome and neurotoxicity due to CAR T cells. *Nat Med* **24**, 739-748 (2018).
21. T. Giavridis *et al.*, CAR T cell-induced cytokine release syndrome is mediated by macrophages and abated by IL-1 blockade. *Nat Med* **24**, 731-738 (2018).
22. S. Chono, T. Tanino, T. Seki, K. Morimoto, Influence of particle size on drug delivery to rat alveolar macrophages following pulmonary administration of ciprofloxacin incorporated into liposomes. *J Drug Target* **14**, 557-566 (2006).
23. O. J. Brady *et al.*, Refining the global spatial limits of dengue virus transmission by evidence-based consensus. *PLoS Negl Trop Dis* **6**, e1760 (2012).
24. J. S. Mackenzie, D. J. Gubler, L. R. Petersen, Emerging flaviviruses: the spread and resurgence of Japanese encephalitis, West Nile and dengue viruses. *Nat Med* **10**, S98-109 (2004).
25. U. C. Chaturvedi, R. Agarwal, E. A. Elbishbishi, A. S. Mustafa, Cytokine cascade in dengue hemorrhagic fever: implications for pathogenesis. *FEMS Immunol Med Microbiol* **28**, 183-188 (2000).
26. S. B. Halstead, E. J. O'Rourke, A. C. Allison, Dengue viruses and mononuclear phagocytes. II. Identity of blood and tissue leukocytes supporting in vitro infection. *J Exp Med* **146**, 218-229 (1977).
27. Y. C. Chen, S. Y. Wang, Activation of terminally differentiated human monocytes/macrophages by dengue virus: productive infection, hierarchical production of innate cytokines and chemokines, and the synergistic effect of lipopolysaccharide. *J Virol* **76**, 9877-9887 (2002).
28. J. Klesney-Tait, I. R. Turnbull, M. Colonna, The TREM receptor family and signal integration. *Nat Immunol* **7**, 1266-1273 (2006).
29. D. N. Cook, D. S. Pisetsky, D. A. Schwartz, Toll-like receptors in the pathogenesis of human disease. *Nat Immunol* **5**, 975-979 (2004).
30. A. P. S. Rathore, A. L. St John, Immune responses to dengue virus in the skin. *Open Biol* **8** (2018).
31. A. S. Pacsa *et al.*, Role of interleukin-12 in patients with dengue hemorrhagic fever. *FEMS Immunol Med Microbiol* **28**, 151-155 (2000).
32. L. Romani, P. Puccetti, F. Bistoni, Interleukin-12 in infectious diseases. *Clin Microbiol Rev* **10**, 611-636 (1997).
33. C. J. Neufeldt *et al.*, SARS-CoV-2 infection induces a pro-inflammatory cytokine response through cGAS-STING and NF-kappaB. *Commun Biol* **5**, 45 (2022).
34. M. Dukhinova, E. Kokinos, P. Kuchur, A. Komissarov, A. Shtro,

Macrophage-derived cytokines in pneumonia: Linking cellular immunology and genetics. *Cytokine Growth Factor Rev* 10.1016/j.cytogfr.2020.11.003 (2020).
35. D. C. Fajgenbaum, C. H. June, Cytokine Storm. *N Engl J Med* **383**, 2255-2273 (2020).
36. I. Julkunen *et al.*, Inflammatory responses in influenza A virus infection. *Vaccine* **19 Suppl 1**, S32-37 (2000).
37. I. Julkunen *et al.*, Molecular pathogenesis of influenza A virus infection and virus-induced regulation of cytokine gene expression. *Cytokine Growth Factor Rev* **12**, 171-180 (2001).
38. K. L. Oslund, N. Baumgarth, Influenza-induced innate immunity: regulators of viral replication, respiratory tract pathology & adaptive immunity. *Future Virol* **6**, 951-962 (2011).
39. M. Merad, J. C. Martin, Pathological inflammation in patients with COVID-19: a key role for monocytes and macrophages. *Nat Rev Immunol* **20**, 355-362 (2020).
40. M. Z. Tay, C. M. Poh, L. Renia, P. A. MacAry, L. F. P. Ng, The trinity of COVID-19: immunity, inflammation and intervention. *Nat Rev Immunol* **20**, 363-374 (2020).
41. K. Shinya *et al.*, Integrated clinical, pathologic, virologic, and transcriptomic analysis of H5N1 influenza virus-induced viral pneumonia in the rhesus macaque. *J Virol* **86**, 6055-6066 (2012).
42. D. Rocksen, B. Lilliehook, R. Larsson, T. Johansson, A. Bucht, Differential anti-inflammatory and anti-oxidative effects of dexamethasone and N-acetylcysteine in endotoxin-induced lung inflammation. *Clin Exp Immunol* **122**, 249-256 (2000).
43. C. Brun-Buisson *et al.*, Early corticosteroids in severe influenza A/H1N1 pneumonia and acute respiratory distress syndrome. *Am J Respir Crit Care Med* **183**, 1200-1206 (2011).
44. M. Giannella *et al.*, Prolonged viral shedding in pandemic influenza A(H1N1): clinical significance and viral load analysis in hospitalized patients. *Clin Microbiol Infect* **17**, 1160-1165 (2011).
45. T. Lammers *et al.*, Dexamethasone nanomedicines for COVID-19. *Nat Nanotechnol* **15**, 622-624 (2020).
46. V. P. Torchilin, Recent advances with liposomes as pharmaceutical carriers. *Nat Rev Drug Discov* **4**, 145-160 (2005).
47. S. Chono, T. Tanino, T. Seki, K. Morimoto, Uptake characteristics of liposomes by rat alveolar macrophages: influence of particle size and surface mannose modification. *J Pharm Pharmacol* **59**, 75-80 (2007).
48. C. Kelly, C. Jefferies, S. A. Cryan, Targeted liposomal drug delivery to monocytes and macrophages. *J Drug Deliv* **2011**, 727241 (2011).
49. S. Tamoutounour *et al.*, CD64 distinguishes macrophages from dendritic cells in the gut and reveals the Th1-inducing role of mesenteric lymph node macrophages during colitis. *Eur J Immunol* **42**, 3150-3166 (2012).
50. J. J. Walsh, L. F. Dietlein, F. N. Low, G. E. Burch, W. J. Mogabgab, Bronchotracheal response in human influenza. Type A, Asian strain,

as studied by light and electron microscopic examination of bronchoscopic biopsies. *Arch Intern Med* **108**, 376-388 (1961).
51. J. K. Taubenberger, D. M. Morens, The pathology of influenza virus infections. *Annu Rev Pathol* **3**, 499-522 (2008).
52. K. B. Walsh *et al.*, Suppression of cytokine storm with a sphingosine analog provides protection against pathogenic influenza virus. *Proc Natl Acad Sci U S A* **108**, 12018-12023 (2011).
53. F. G. Hayden *et al.*, Local and systemic cytokine responses during experimental human influenza A virus infection. Relation to symptom formation and host defense. *J Clin Invest* **101**, 643-649 (1998).
54. W. Kozak *et al.*, Sickness behavior in mice deficient in interleukin-6 during turpentine abscess and influenza pneumonitis. *Am J Physiol* **272**, R621-630 (1997).
55. L. Kaiser, R. S. Fritz, S. E. Straus, L. Gubareva, F. G. Hayden, Symptom pathogenesis during acute influenza: interleukin-6 and other cytokine responses. *J Med Virol* **64**, 262-268 (2001).
56. M. Bartneck *et al.*, Liposomal encapsulation of dexamethasone modulates cytotoxicity, inflammatory cytokine response, and migratory properties of primary human macrophages. *Nanomedicine* **10**, 1209-1220 (2014).
57. A. F. Belgaumi *et al.*, Dexamethasone-associated toxicity during induction chemotherapy for childhood acute lymphoblastic leukemia is augmented by concurrent use of daunomycin. *Cancer* **97**, 2898-2903 (2003).
58. G. Palladini *et al.*, The combination of thalidomide and intermediate-dose dexamethasone is an effective but toxic treatment for patients with primary amyloidosis (AL). *Blood* **105**, 2949-2951 (2005).
59. G. Palladini *et al.*, Association of melphalan and high-dose dexamethasone is effective and well tolerated in patients with AL (primary) amyloidosis who are ineligible for stem cell transplantation. *Blood* **103**, 2936-2938 (2004).
60. R. Anderson *et al.*, Liposomal encapsulation enhances and prolongs the anti-inflammatory effects of water-soluble dexamethasone phosphate in experimental adjuvant arthritis. *Arthritis Res Ther* **12**, R147 (2010).
61. J. Kroon *et al.*, Liposomal delivery of dexamethasone attenuates prostate cancer bone metastatic tumor growth in vivo. *Prostate* **75**, 815-824 (2015).
62. A. T. Back, A. Lundkvist, Dengue viruses - an overview. *Infect Ecol Epidemiol* **3** (2013).
63. J. Khan, A. Ghaffar, S. A. Khan, The changing epidemiological pattern of Dengue in Swat, Khyber Pakhtunkhwa. *PLoS One* **13**, e0195706 (2018).
64. S. Bhatt *et al.*, The global distribution and burden of dengue. *Nature* **496**, 504-507 (2013).
65. P. Avirutnan *et al.*, Vascular leakage in severe dengue virus infections: a potential role for the nonstructural viral protein NS1 and complement. *J Infect Dis* **193**, 1078-1088 (2006).

66. G. N. Malavige *et al.*, Cellular and cytokine correlates of severe dengue infection. *PLoS One* **7**, e50387 (2012).
67. J. N. Mangione *et al.*, The association of cytokines with severe dengue in children. *Trop Med Health* **42**, 137-144 (2014).
68. A. L. Rothman, Immunity to dengue virus: a tale of original antigenic sin and tropical cytokine storms. *Nat Rev Immunol* **11**, 532-543 (2011).
69. D. A. Vignali, V. K. Kuchroo, IL-12 family cytokines: immunological playmakers. *Nat Immunol* **13**, 722-728 (2012).
70. F. Brombacher, R. A. Kastelein, G. Alber, Novel IL-12 family members shed light on the orchestration of Th1 responses. *Trends Immunol* **24**, 207-212 (2003).
71. M. H. Lexberg *et al.*, IFN-gamma and IL-12 synergize to convert in vivo generated Th17 into Th1/Th17 cells. *Eur J Immunol* **40**, 3017-3027 (2010).
72. H. Shirota, M. Gursel, D. M. Klinman, Suppressive oligodeoxynucleotides inhibit Th1 differentiation by blocking IFN-gamma- and IL-12-mediated signaling. *J Immunol* **173**, 5002-5007 (2004).
73. C. Sgadari, A. L. Angiolillo, G. Tosato, Inhibition of angiogenesis by interleukin-12 is mediated by the interferon-inducible protein 10. *Blood* **87**, 3877-3882 (1996).
74. E. E. Voest *et al.*, Inhibition of angiogenesis in vivo by interleukin 12. *J Natl Cancer Inst* **87**, 581-586 (1995).
75. W. Lasek *et al.*, Antitumor effects of the combination immunotherapy with interleukin-12 and tumor necrosis factor alpha in mice. *Cancer Immunol Immunother* **45**, 100-108 (1997).
76. S. Mitola, M. Strasly, M. Prato, P. Ghia, F. Bussolino, IL-12 regulates an endothelial cell-lymphocyte network: effect on metalloproteinase-9 production. *J Immunol* **171**, 3725-3733 (2003).
77. U. C. Chaturvedi, R. Nagar, R. Shrivastava, Macrophage and dengue virus: friend or foe? *Indian J Med Res* **124**, 23-40 (2006).
78. A. Torrentes-Carvalho *et al.*, Dengue-2 infection and the induction of apoptosis in human primary monocytes. *Mem Inst Oswaldo Cruz* **104**, 1091-1099 (2009).
79. J. L. Miller *et al.*, The mannose receptor mediates dengue virus infection of macrophages. *PLoS Pathog* **4**, e17 (2008).
80. M. F. Wu *et al.*, CLEC5A is critical for dengue virus-induced inflammasome activation in human macrophages. *Blood* **121**, 95-106 (2013).
81. D. M. Morens, Antibody-dependent enhancement of infection and the pathogenesis of viral disease. *Clin Infect Dis* **19**, 500-512 (1994).
82. R. Littaua, I. Kurane, F. A. Ennis, Human IgG Fc receptor II mediates antibody-dependent enhancement of dengue virus infection. *J Immunol* **144**, 3183-3186 (1990).
83. T. Oliphant *et al.*, Antibody recognition and neutralization determinants on domains I and II of West Nile Virus envelope protein. *J Virol* **80**, 12149-12159 (2006).

84. T. Oliphant *et al.*, Development of a humanized monoclonal antibody with therapeutic potential against West Nile virus. *Nat Med* **11**, 522-530 (2005).
85. E. Pokidysheva *et al.*, Cryo-EM reconstruction of dengue virus in complex with the carbohydrate recognition domain of DC-SIGN. *Cell* **124**, 485-493 (2006).
86. S. T. Chen *et al.*, CLEC5A is critical for dengue-virus-induced lethal disease. *Nature* **453**, 672-676 (2008).
87. R. M. Zellweger, T. R. Prestwood, S. Shresta, Enhanced infection of liver sinusoidal endothelial cells in a mouse model of antibody-induced severe dengue disease. *Cell Host Microbe* **7**, 128-139 (2010).
88. S. Goriely *et al.*, Human IL-12(p35) gene activation involves selective remodeling of a single nucleosome within a region of the promoter containing critical Sp1-binding sites. *Blood* **101**, 4894-4902 (2003).
89. S. I. Gringhuis *et al.*, C-type lectin DC-SIGN modulates Toll-like receptor signaling via Raf-1 kinase-dependent acetylation of transcription factor NF-kappaB. *Immunity* **26**, 605-616 (2007).
90. J. Liu, S. Cao, L. M. Herman, X. Ma, Differential regulation of interleukin (IL)-12 p35 and p40 gene expression and interferon (IFN)-gamma-primed IL-12 production by IFN regulatory factor 1. *J Exp Med* **198**, 1265-1276 (2003).
91. Y. L. Lo *et al.*, Dengue Virus Infection Is through a Cooperative Interaction between a Mannose Receptor and CLEC5A on Macrophage as a Multivalent Hetero-Complex. *PLoS One* **11**, e0166474 (2016).
92. P. S. Sung, S. L. Hsieh, CLEC2 and CLEC5A: Pathogenic Host Factors in Acute Viral Infections. *Front Immunol* **10**, 2867 (2019).
93. J. Ruland, L. Hartjes, CARD-BCL-10-MALT1 signalling in protective and pathological immunity. *Nat Rev Immunol* **19**, 118-134 (2019).
94. V. Landre, E. Pion, V. Narayan, D. P. Xirodimas, K. L. Ball, DNA-binding regulates site-specific ubiquitination of IRF-1. *Biochem J* **449**, 707-717 (2013).
95. S. Kalayanarooj, Clinical Manifestations and Management of Dengue/DHF/DSS. *Trop Med Health* **39**, 83-87 (2011).
96. S. Ubol, W. Phuklia, S. Kalayanarooj, N. Modhiran, Mechanisms of immune evasion induced by a complex of dengue virus and preexisting enhancing antibodies. *J Infect Dis* **201**, 923-935 (2010).
97. D. H. Libraty *et al.*, High circulating levels of the dengue virus nonstructural protein NS1 early in dengue illness correlate with the development of dengue hemorrhagic fever. *J Infect Dis* **186**, 1165-1168 (2002).
98. S. Ben Mkaddem, M. Benhamou, R. C. Monteiro, Understanding Fc Receptor Involvement in Inflammatory Diseases: From Mechanisms to New Therapeutic Tools. *Front Immunol* **10**, 811 (2019).
99. K. M. Dennehy *et al.*, Syk kinase is required for collaborative cytokine production induced through Dectin-1 and Toll-like

receptors. *Eur J Immunol* **38**, 500-506 (2008).
100. I. Zanoni *et al.*, CD14 controls the LPS-induced endocytosis of Toll-like receptor 4. *Cell* **147**, 868-880 (2011).
101. J. Y. Yang *et al.*, ERK promotes tumorigenesis by inhibiting FOXO3a via MDM2-mediated degradation. *Nat Cell Biol* **10**, 138-148 (2008).
102. Y. Haupt, R. Maya, A. Kazaz, M. Oren, Mdm2 promotes the rapid degradation of p53. *Nature* **387**, 296-299 (1997).
103. C. A. Hunter, New IL-12-family members: IL-23 and IL-27, cytokines with divergent functions. *Nat Rev Immunol* **5**, 521-531 (2005).
104. J. P. Leonard *et al.*, Effects of single-dose interleukin-12 exposure on interleukin-12-associated toxicity and interferon-gamma production. *Blood* **90**, 2541-2548 (1997).
105. A. Hunziker, M. H. Jensen, S. Krishna, Stress-specific response of the p53-Mdm2 feedback loop. *BMC Syst Biol* **4**, 94 (2010).
106. T. Venkatesan *et al.*, MDM2 Overexpression Modulates the Angiogenesis-Related Gene Expression Profile of Prostate Cancer Cells. *Cells* **7** (2018).

국문 초록

마크로파지는 숙주의 방어와 세균, 바이러스, 진균을 포함한 외부 미생물에 대한 면역에 현저하게 관여하는 여러 기능을 가진 타고난 세포 면역의 중요한 구성 요소이다. 많은 바이러스가 마크로파지를 표적으로 하고, 활성화된 마크로파지는 식세포작용을 일으키며 염증성 사이토카인과 케모카인을 분비한다. 그러나 마크로파지에 의한 염증 유발 사이토카인의 과도한 분비는 국소 조직 손상과 위험한 전신 염증 반응에 기여한다. 단핵구와 마크로파지는 염증성 사이토카인을 분비하는 주요 세포이기 때문에 이러한 세포의 효율적인 제어는 사이토카인을 조절하는 치료 표적으로 사용될 수 있다. 본 연구에서는 마크로파지를 표적으로 하여 인플루엔자 바이러스 매개 염증 반응을 조절하고, 이후 뎅기 바이러스 감염 시 마크로파지에서 특이적으로 IL-12를 조절하는 면역 기전을 조사하고자 하였다. 첫번째로, 본 연구는 마크로파지에 선택적으로 전달이 되는 리포솜을 개발하였다. 이후 인플루엔자 바이러스 감염 마우스 모델에서 덱사메타손 리포솜을 전달 했을 때 TNF-α, IL-1β, IL-6, CXCL2와 같은 염증성 사이토카인, 케모카인이 감소하고, 침윤된 염증성 세포를 감소된다는 것을 밝혔다. 이로 인해 질병이 진행되는 동안 덱사메타손 리포솜 치료는 사망률을 20%까지 감소시켰다. 결과적으로 덱사메타손 리포솜의 비강 내 전달은 인플루엔자 바이러스 매개 폐렴의 치료를 위한 유망한 치료 전략으로 작용할 수 있음을 시사한다 (Chapter 1). 다음으로 마크로파지에 심각한 뎅기 바이러스 감염 후 IL-12가 감소하는 원인을 뎅기 바이러스 결합 수용체 매개 신호전달을 통해 밝혀냈다. 그 결과, IFNAR KO 마우스가 중증 뎅기 바이러스에 감염된 경우, 감소된 IL-12가 MMP-9를 증가시켜 혈관 투과성을 증가시킨다는 것을 밝혔다. 또한, 재조합 IL-12로

치료한 마우스가 체중을 빠르게 회복하고 뎅기출혈열을 완화시키는 것을 밝혔다. 본 연구에서는 뎅기출혈열을 억제할 수 있는 잠재적인 치료 전략을 제시하였다 (Chapter 2). 결론적으로 본 연구는 마크로파지를 표적으로 하여 사이토카인을 조절함으로써 바이러스에 대한 면역 요법의 치료적 접근에 중요한 근거 자료로 사용할 수 있을 것으로 기대된다.

키워드: 마크로파지, 면역치료, 인플루엔자 바이러스, 뎅기 바이러스, 사이토카인, 리포솜

학번: 2016-21898